

The milankovitch fingerprint on the distribution and thickness of bedding-parallel veins (beef) in source rocks

E. Ravier, Mathieu Martinez, Pierre Pellenard, Alain Zanella, Lucie Tupinier

▶ **To cite this version:**

E. Ravier, Mathieu Martinez, Pierre Pellenard, Alain Zanella, Lucie Tupinier. The milankovitch fingerprint on the distribution and thickness of bedding-parallel veins (beef) in source rocks. Marine and Petroleum Geology, 2020, 122, pp.104643. 10.1016/j.marpetgeo.2020.104643 . insu-02922274

HAL Id: insu-02922274

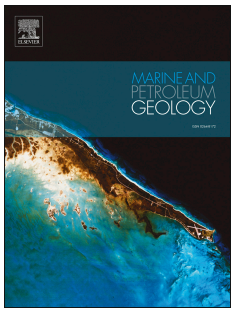
https://insu.hal.science/insu-02922274

Submitted on 26 Aug 2020

HAL is a multi-disciplinary open access archive for the deposit and dissemination of scientific research documents, whether they are published or not. The documents may come from teaching and research institutions in France or abroad, or from public or private research centers.

L'archive ouverte pluridisciplinaire **HAL**, est destinée au dépôt et à la diffusion de documents scientifiques de niveau recherche, publiés ou non, émanant des établissements d'enseignement et de recherche français ou étrangers, des laboratoires publics ou privés.

Journal Pre-proof



The milankovitch fingerprint on the distribution and thickness of bedding-parallel veins (beef) in source rocks

Edouard Ravier, Mathieu Martinez, Pierre Pellenard, Alain Zanella, Lucie Tupinier

PII: S0264-8172(20)30426-8

DOI: https://doi.org/10.1016/j.marpetgeo.2020.104643

Reference: JMPG 104643

To appear in: *Marine and Petroleum Geology*

Received Date: 16 April 2020

Revised Date: 3 July 2020

Accepted Date: 3 August 2020

Please cite this article as: Ravier, E., Martinez, M., Pellenard, P., Zanella, A., Tupinier, L., The milankovitch fingerprint on the distribution and thickness of bedding-parallel veins (beef) in source rocks, *Marine and Petroleum Geology* (2020), doi: https://doi.org/10.1016/j.marpetgeo.2020.104643.

This is a PDF file of an article that has undergone enhancements after acceptance, such as the addition of a cover page and metadata, and formatting for readability, but it is not yet the definitive version of record. This version will undergo additional copyediting, typesetting and review before it is published in its final form, but we are providing this version to give early visibility of the article. Please note that, during the production process, errors may be discovered which could affect the content, and all legal disclaimers that apply to the journal pertain.

© 2020 Published by Elsevier Ltd.

Journal Pre-proof

Credit author statement

Edouard Ravier: conceptualization, investigation, visualization, writing original draft

Mathieu Martinez: conceptualization, methodology, investigation, formal analysis, writing original draft

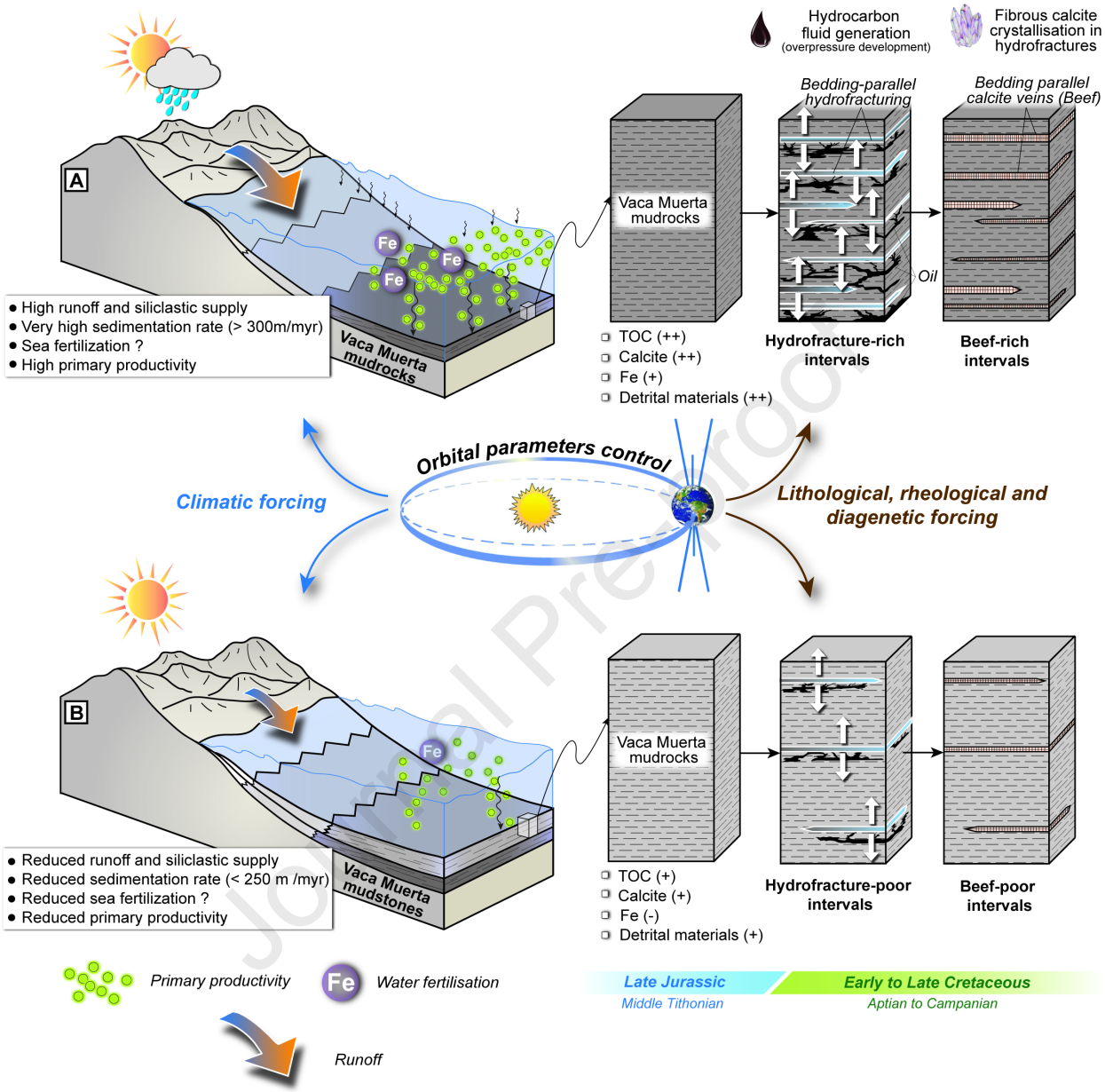
Pierre Pellenard : conceptualization, methodology, review and editing

Alain Zanella : conceptualization, investigation, review and editing

Lucie Tupinier : investigation, formal analysis

Journal Pre-proof

Journal Pre-proof



Journal Pre-proof

The Milankovitch fingerprint on the distribution and thickness of bedding-parallel veins (beef) in source rocks

Edouard Ravier[a], Mathieu Martinez[b], Pierre Pellenard[c], Alain Zanella[a], Lucie Tupinier[c]

a. Le Mans Université, Géosciences Le Mans - LPG UMR 6112, 72085 Le Mans, France

b. Univ Rennes, CNRS, Géosciences Rennes - UMR 6118, F-35000 Rennes, France

c. Biogéosciences, UMR CNRS/uB 6282, Université Bourgogne Franche-Comté, F–21000 Dijon, France

Abstract

Bed-parallel, mineralized fractures are common in source rocks and generally consist in mm to cm thick veins developed parallel to bedding known as beef or bedding-parallel veins. Considering they can form a dense network of mechanical discontinuities, the prediction of beef distribution is a major issue impacting shale reservoir production. Beef distribution is predominantly controlled by the lithological characteristics of source rocks and we here decipher the relation between mineralogical and chemical proxies controlled by orbital parameters and distribution of the beef along a Late Jurassic section of the well-known Vaca Muerta Formation source rock in the Neuquén Basin. Using multiple proxies collected along the beef-rich Huncal section, we show that Milankovitch cycles rule the mineralogical evolution and beef distribution in these organic-rich mudrocks. Cycles inferred from the statistical treatment of sedimentary (magnetic susceptibility, elemental and mineralogical ratios), biogenic (total organic carbon) and diagenetic (beef distribution and thickness) signals revealed indeed the influence of an astroclimatic fingerprint in sediments and on processes controlling mineralized fracture generation and distribution. The astroclimatic memory

Journal Pre-proof

recorded in many source rocks worldwide is therefore envisaged as a suitable proxy for the prediction of mineralized fracture distribution.

Keywords: beef; bedding-parallel veins; Milankovitch cycles; astroclimatic forcing; diagenesis; source rocks.

Corresponding author: Edouard Ravier; Edouard.ravier@univ-lemans.fr

1. Introduction

During burial and diagenesis, sediments can reach a state of overpressure at depth when the pore fluid pressure becomes greater than that of an equivalent free column of water (hydrostatic pressure). The burial of organic-rich mudrock (e.g., source rock) is commonly associated with the development of fluid overpressures due to mechanical and chemical compaction of clay and thermal maturation of kerogen (Grauls, 1997; Swarbrick et al., 2002; Cobbold and Rodrigues, 2007). The release of water and genesis of oil and gas within low-permeability source rocks is responsible for a drastic increase of their pore-fluid pressure. In response to this distributed overpressure, hydrofractures can develop parallel to bedding (Cosgrove, 1995; Rodrigues et al., 2009; Gale et al., 2014; Zhang et al., 2016). The occurrence of bedding parallel fibrous veins in source rocks has commonly been interpreted as the mineralisation of such hydrofractures (Cobbold et al., 2013). These veins, also referred to as beef or Bedding-Parallel Veins (BPV), are mostly composed of fibrous calcite although gypsum or quartz veins have been described in the literature (Cobbold et al., 2013 and references therein). Inclusions of either liquid (oil) or solid (bitumen) hydrocarbons in the veins illustrate the relative synchronicity between kerogene cracking, hydrofracturing and

Journal Pre-proof

precipitation of supersaturated aqueous solutions (Rodrigues et al., 2009; Zanella et al., 2015b). The occurrence of BPV in organic-rich sediment of low maturity has also led to suggest that beef may be produced during sediment degassing and/or rapid deposition of the overlying sediments or by the combination of pressure solution and the driving force of crystallization (Meng et al., 2017, 2018). The common occurrence of BPVs in foreland basins worldwide suggests that their formation is often a consequence of both fluid overpressures and compressional tectonic stress (Zanella et al., 2020).

Some organic-rich sediments display intervals with very high beef concentration. The Jurassic-Cretaceous black shales of the Vaca Muerta Formation (Argentina) or the Charmouth Mudstone Formation with the so-called “Shales-with-beef Member” (England) are among the best examples of section gathering tens of closely-spaced horizontal and fibrous calcite veins (Rodrigues et al., 2009; Zanella et al., 2015a,b; Meng et al., 2017). Beef can reach up to 10% of the rock volume for some intervals of the Vaca Muerta Fm in the Huncal area, with thickness ranging from a few millimeters to 16 centimeters for individualBPVs (Rodrigues et al., 2009). Weger et al (2019) provided a high-resolution logging of beef distribution in a 800 meters thick section of Vaca Muerta Formation (Puerta Curaco area) and showed that more than 50 meters of the section contains an excess of 2% beef measured by percentage of rock volumes. Similarly, Lejay et al (2017) estimated a proportion of 2 to 3% of beef throughout the Vaca Muerta Fm using core data from the eastern part of the Neuquén basin.

Knowing that mineralized fractures behave as major mechanical discontinuities in source rocks and influence both hydraulic fracture stimulation and production (Gale et al., 2014), the prediction of beef distribution is therefore a major issue as many studies aim to better constrain the mechanical properties of source rocks. The location, distribution and thickness of BPV are thought to be organized and controlled by several parameters related to the total organic carbon in sediments, the maturation of organic matter, the nature and content of

Journal Pre-proof

carbonate and any types of rheological heterogeneities in the host rock that could alter its geomechanics and provide space or a nucleus for carbonate precipitation (Gale et al., 2014; Lejay et al., 2017; Meng et al., 2017, 2018). These parameters are mainly inherited from palaeoenvironmental conditions during mudstone deposition because the grain-size, mineralogy and organic content of sediments are most often related to the combination of climatic and eustatic variations, especially for organic-rich sediments from a marine origin. Some correlations (sometimes very weak) between beef distribution and ash beds or diagenetic concretions described in some parts of the Neuquén Basin implies that rheological heterogeneities and mechanical contrast in mudstone can also be related to the local imprint of aerial explosive volcanism or to the superimposed diagenetic signature for examples (Lejay et al., 2017; Weger et al, 2019).

The Earth experiences periodic changes in the eccentricity, inclination and orientation of the Ecliptic plane as well as periodic motions of its rotational axis (see also Hinnov, 2018 for a review). The orbital parameters resulting from these motions are: (i) the eccentricity, which is the change of the shape of the Ecliptic plane from the perfect circle to an ellipse. The eccentricity cycles have main periods of ~100 kyr, 405 kyr and 2.4 Myr (Laskar et al., 2011); (ii) the obliquity, which is the angle between the perpendicular to the Ecliptic plane and the Earth's rotational axis. The obliquity cycles have a main period calculated at 38.0 ± 1.7 kyr in the Tithonian (Waltham, 2015) and (iii) the climatic precession, which corresponds to the drift of the Earth-Sun distance at a given date of the year. The climatic precession cycles have an average period calculated at 20.2 ± 0.5 kyr in the Tithonian (Waltham, 2015). These orbital parameters modify cyclically the difference in insolation between summer and winter at a given latitude. The change in the seasonal difference in insolation then affects the oceanic and atmospheric circulations, the amount of water evaporated above the ocean and precipitated above the landmasses, the vegetation and ice covers, the sea level, the weathering intensity,

Journal Pre-proof

the detrital and nutrient supply to marine environments, the primary productivity, the redox conditions and, finally, the preservation of organic matter (Strasser, 2006). All these orbital imprints then may impact the petrophysical and mechanical properties of the sediment deposited and influence the evolution of the sediment during the burial diagenesis.

Considering that both climate and sea-level oscillations are partly controlled by Milankovitch cyclicity, we aim to decipher if the distribution and thickness of mineralized hydrofractures (e.g., beef) in organic-rich sediments are indirectly forced by cyclic astroclimatic changes. This hypothesis, if confirmed, could help predict the distribution of BPVs in organic-rich mudrock using the well-calibrated record of astronomical cycles.

In the Vaca Muerta Fm. of the Neuquén Basin, sedimentological, mineralogical and chemical studies pointed the role of the orbital forcing in humid/arid and sea-level cycles which generated marl-limestone alternations (Scasso et al., 2005; Kietzmann et al., 2011, 2015). In particular, annually humid conditions favoured detrital input to the basin and led to the deposits of siltstone and claystone while limestone beds originate from the export of carbonate mud to the basin under semi-arid conditions (Scasso et al., 2005; Rodriguez Blanco et al., 2020). Humid conditions and increased nutrient input favoured, together with increased sea level, the primary productivity in the basin and the preservation of organic matter (Scasso et al., 2005; Kietzmann et al., 2015). The sedimentary record of orbital cycles has thereby already been recognized in the Late Jurassic and Early Cretaceous deposits of the Neuquén Basin from bed pattern, geochemistry, and magnetic susceptibility (Scasso et al., 2005; Kietzmann et al., 2015; Kohan-Martinez et al., 2018; Kietzmann et al., 2018; Aguirre-Urreta et al., 2019). The Neuquén basin appears especially suitable to investigate the relationship between astroclimatic forcing and distribution/thickness of mineralized palaeo-hydrofractures. To document this potential forcing, we revisited the Huncal section of the Upper Jurassic - Lower Cretaceous Vaca Muerta Fm in the Neuquén Basin containing a high beef

Journal Pre-proof

concentration (Rodrigues et al., 2009; Larmier, 2020). This outcrop displays a continuous sedimentary record composed of overmatured organic-rich black shales interbedded with abundant bedding-parallel calcite veins (. A coupled analysis of sedimentary proxies and of the palaeo-hydrofracturing signal has therefore been conducted using high-resolution measurements of Magnetic Susceptibility (MS), Total Organic Carbon (TOC), mineralogical (bulk and clay size fraction) and chemical composition together with beef distribution and thickness. Spectral analyses have been applied to all proxies in order to test and compare their potential cyclicity in relation with astronomical cycles and beef distribution/thickness and to conclude about the impact of orbitally-driven climate changes on diagenesis and fracture distribution in relation with the primary paleoenvironmental signal.

2. Geological context

2.1. The Neuquén Basin

The Neuquén Basin has a broadly triangular shape and is located in the Western part of Argentina, in the foreland and foothills of the Andes (Fig. 1A) (Howell et al., 2005). The Neuquén Basin was a retro-arc basin developed during the Mesozoic at the Pacific margin of South America (Legarreta and Uliana, 1991). The basin is filled by an Upper Triassic to Upper Cenozoic sedimentary succession that includes continental and marine siliciclastic sediments, carbonates and evaporites deposited during the different stages of the basin evolution. From the Upper Triassic to the Lower Jurassic deposits, narrow and isolated depocentres composed of continental and volcanic deposits accumulated during the extensional regime phase (Vergani et al., 1995; Franzese and Spalletti, 2001; Ramos et al., 2019). From the Lower Jurassic to the Upper Cretaceous deposits, regional thermal

Journal Pre-proof

subsidence related to the subduction along the western margin of the basin is responsible for a wide marine embayement (up to 4000 m deep) recorded as marine deposits that shallow up eastwards and a fringe of continental deposits on the outer margin of the basin (Vergani et al., 1995). From the Upper Cretaceous to the Upper Cenozoic deposits, a thick succession of synorogenic continental sediments filled the basin during compressive deformation regime (Legarreta and Uliana, 1991). This Andean deformation phase resulted in the development of fold and thrust belts that exhumed Mesozoic succession throughout the basin (Fig. 1A).

2.2. The Vaca Muerta Formation

Outstanding Upper Jurassic to Lower Cretaceous outcrops are exposed in the basin, especially in the western central part of the basin where the Tithonian-early Valanginian interval is recorded through a sedimentary pile locally reaching 1500 m thick (Leanza et al., 2011). This Upper Jurassic to Lower Cretaceous sequence is composed of transgressive-regressive sequences that developed in response to variations in subsidence rate, eustatic fluctuations and regional uplift (Legarreta and Gulisano, 1989; Kietzmann et al., 2014; Krim et al., 2017). These marine sequences are included in the Mendoza Group (also referred to as Mendoza Mesosequence) (Fig. 1C). Legarreta and Gulisano (1989) divided the Mendoza Group into three shallowing upward sedimentary sequences: the lower Mendoza Subgroup (Kimmeridgian–Lower Valanginian), the middle Mendoza Subgroup (Upper Valanginian-Lower Hauterivian) and the upper Mendoza Subgroup (Upper Hauterivian–Lower Barremian). The lower Mendoza Subgroup, object of the present study, records the continental deposits of the Tordillo Formation (Kimmeridgian-lower part of the Lowermost Tithonian) and the thick deep marine deposits of the Vaca Muerta Fm (upper part of the Lower Tithonian - Upper Berriasian to Lower Valanginian) (Figs. 1B, C). In most areas of the

Journal Pre-proof

Neuquén Basin, the Vaca Muerta Fm corresponds to dark and organic-rich mudrocks, marls and limestones deposited along a homoclinal ramp flooded by a marine transgression originating from the Pacific Ocean (Kietzmann et al., 2014). The Vaca Muerta black shales are basinal ramp facies considered as a world-class source rock (with TOC values ranging from 2 to 12%) of high unconventional hydrocarbon potential . The Vaca Muerta Fm is diachronous as the top becomes younger toward the central part of the basin (Leanza et al., 2003). In the western part of the Vaca Muerta Fm, a Lower Berriasian turbiditic sandstone interval referred to as the Huncal Member is a useful stratigraphic marker (Leanza et al., 2003) (Figs. 1 B, C; 2A).

Journal Pre-proof

Journal Pre-proof

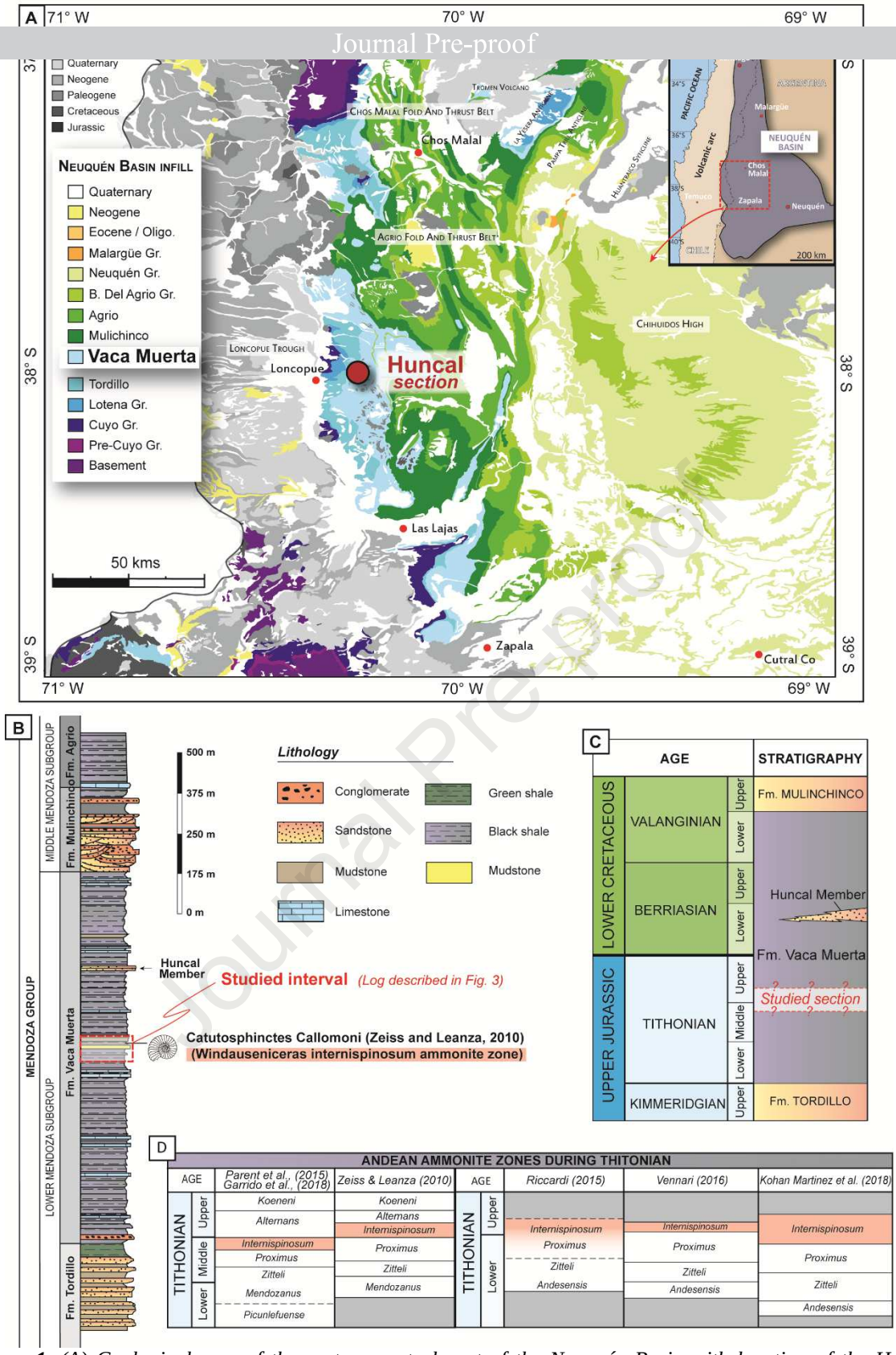


Figure 1. *(A) Geological map of the eastern central part of the Neuquén Basin with location of the Huncal section. (B) Section of the Vaca Muerta Fm in the Huncal area (modified after Leanza et al., 2003) with a focus on the position of the sedimentary interval described in this study. (C) Lithostratigraphic framework of the Vaca Muerta Fm in the Huncal area (modified after Leanza et al., 2011). (D) Chart of the Tithonian ammonoid biostratigraphy for the Andean region based on multiple studies conducted in the Neuquén Basin.*

Journal Pre-proof

194

195 *2.3. The Huncal section*

196

197 The section investigated in this study, belonging to the Vaca Muerta Fm, is located near the
198 locality of Huncal, along the Huncal river, a few kilometers southeast of Cerro Mulinchinco
199 (38°06.242' S; O 70°35.847' W) (Fig. 1A). A synthetic log of the Huncal area has been
200 realised by Leanza et al. (2011), where a complete 1150 m thick section of the Vaca Muerta
201 Fm is reported (Fig. 1B). Leanza's work conducted in this area refers to a beef-rich interval
202 approximately 250 m beneath the Huncal Mb, especially in the area of Cerro Mulinchinco
203 (Leanza et al., 2003, 2011). We studied a 102 m thick and continuous section that shows a
204 very high beef concentration we highly suspect to be the equivalent of the "shales with beef"
205 interval described in Leanza et al. (2011). The beef-rich section we investigated is beneath the
206 Huncal Mb (Figs. 1B, C; 2A). Ammonites are commonly found along the section and best
207 preserved in bedding-parallel calcite veins (Rodrigues et al., 2009). Although mostly
208 degraded, one ammonite specimen identified in the uppermost part of the section corresponds
209 to *Catutosphinctes Callomoni* (H. Leanza pers. comm.) (Figs. 1B, 2C; 3). According to Zeiss
210 and Leanza (2010), this species is characteristic of the *Windauseniceras internispinosum*
211 Andean ammonite Zone, indicating a Middle to early Upper Tithonian age (Fig. 1D).
212 Recently, astronomical calibration of the Tithonian-Berriasian conducted in the Neuquén
213 Basin has estimated to 1.21 myr the duration of the *W. internispinosum* Zone (Kietzmann et
214 al., 2018).

215

216 *2.4 Bedding-parallel calcite veins (beef) in the Huncal area*

217

218 BPV or beef have been largely studied in the Vaca Muerta Fm due to their widespread
219 occurrence in the Neuquén Basin (Rodrigues et al., 2009; Gale et al., 2014; Zanella et al.,

Journal Pre-proof

2015b; Eberli et al., 2017; Lejay et al., 2017; Ukar et al., 2017; Weger et al., 2019). Typical veins are composed of fibrous calcite perpendicular to bedding that are either continuous, discontinuous or lens-shaped. They commonly display several generations of calcite crystallisation related to several phases of hydrofractures opening along a single mechanic interface. The inner generations are generally grey, as a result of numerous inclusions of wall rock and hydrocarbons. The outer generations are white, because of a lack of these inclusions. A median line or zone appears between the inner zones. This line also contains abundant inclusions of wall rock (Rodrigues et al., 2009). From burial curves, maturity calculations, growth strata, and ages of igneous intrusions, Rodrigues et al. (2009) estimated that the inner generation of the beef formed when the formation reached the oil window during the Aptian-Albian. Conversely, the outer generation formed when the formation reached the gas window during the Cenomanian-Campanian. Their formation is attributed to organic matter abundance in black shales and fluid overpressure development during chemical compaction and transformation of solid kerogen into oil or gas (Rodrigues, 2009). Larmier (2020) demonstrated the link between TOC and beef characteristics along the studied section by showing highest density of beef in sedimentary intervals displaying higher TOC values. Nevertheless, this relationship between TOC and beef occurence is not always recorded in the basin (Weger et al., 2019).

3. Materials and Methods

3.1. Sampling and methodology for beef position and thickness

We conducted a high-resolution sedimentary logging and sampling along a 100 m thick section in the Huncal area. Using a Jacob's staff, a 1:10 sedimentary logging has been carried

Journal Pre-proof

together with an even sampling step of 10 cm (1000 samples in total). Beef layers and dolostone beds were discarded from the measurement of the sampling distances to only sample shales and eliminate any bias in the physical and chemical signals acquired. In parallel, maximum thickness and lateral continuity of every beef have been measured. The outcrop generally offered tens of meters long viewing of single beef, a rough estimation of the degree of continuity was therefore performed by observing their lateral continuity at outcrop scale. Continuous beef at outcrop scale were therefore labelled as "continuous" while beef with poor lateral continuity or lens-shaped were labelled as "discontinuous". Diffuse beef less than a millimeter-thick, referred to as "microbeef" in some studies (Lejay et al., 2017; Larmier, 2020) were very difficult to fully characterize and were therefore not measured.

To quantify the beef signal along the section, we extracted three signals from the beef database: (1) beef occurrence, (2) beef median line position and (3) beef thickness. (1) Beef occurrence corresponds to the beef presence or absence for every single millimeter of the section. A value of 1 is attributed to the presence of beef while a value of 0 corresponds to mm-thick intervals devoid of beefs. (2) The beef median line position corresponds to the position of the median line (Fig. 4B) of every single beef described along the section. (3) The beef thickness signal required an additional operation to be independent from the occurrence or median line signals described above. The beef thickness values are resampled every 10 cm along a curve constituted by a point-to-point linear interpolation between thickness values recorded for every beef position. As the very few thick beefs occurring in beef-poor intervals bring a substantial bias in the interpolation curve (see section 4.7), we built an additional curve where they have been removed.

3.2. Magnetic Susceptibility

Journal Pre-proof

Magnetic susceptibility (MS) was measured on the 1000 bulk shale samples collected every 10 cm along the section to analyse the evolution of the detrital export along the section. Usually, iron bearing minerals have higher magnetic susceptibility values than non-iron bearing minerals. As the iron is exported to the basin from the continental erosion and weathering, MS measurements will help deciphering the impact of the Milankovitch cycles on the detrital export. MS values were acquired using a laboratory Agico Kappabridge KLY-3S samples (Geosciences Rennes, Université Rennes 1). Volumic MS was measured three times and corrected from measurements of volumic MS performed on empty containers. Sample values, corrected from blanks, were normalized to the measurement volume and the sample mass and given in m^3/kg.

3.3. Total Organic Carbon

We used 198 samples collected for MS measurements for to TOC measurements (in % weight) following an even sampling step of 50 cm. Both organic carbon content and thermal maturation of the organic matter were measured using a Rock-Eval instrument (Rock-Eval 6 Turbo device; Vinci Technologies). TOC results from this sampling series along the Huncal section have already been published in Larmier (2020).

3.4. X-ray diffraction

X-ray diffraction (XRD) analyses were conducted on 30 shale samples every 3 meters along the section to obtain the whole mineralogical composition. The first 33 meters, corresponding to a beef-rich stratigraphic interval (Fig. 3), has been selected for higher resolution XRD analyses with samples measured every 30 cm (100 samples in total).

Journal Pre-proof

Each sample was cleaned, crushed and finely powdered using a metal ring grinder. Diffractograms were obtained using a Bruker D4 Endeavor diffractometer with CuK_{α} radiations, LynxEye detector and a Ni filter, under 40 kV voltage and 25 mA intensity (Biogéosciences Laboratory, Université Bourgogne Franche-Comté). The goniometer scanned the sample from 2.5° to 30° for each run showing diffraction peaks for every crystalized mineral phase.

Minerals phases were identified by the position of their main diffraction peaks while semi-quantitative estimates were produced in relation to their area (Moore and Reynolds, 1997). Areas were determined on diffractograms with MacDiff 4.2.5 software (Petschick, 2000). Beyond the evaluation of the absolute proportions, the objective is to identify their relative fluctuations along the section. Peak area ratios were then considered for time series analyses. Clay mineral identification and semi-quantification were also performed on the decarbonated clay-sized fraction (<2µm) using a 0.2 M HCl solution. Three runs were performed for each sample to discriminate clay phases using oriented glass slide preparation: 1) air-drying; 2) ethylene-glycol solvation; 3) heating at 490 °C. Clay minerals were identified using their main diffraction (d_{001}) peak and by comparing the three diffractograms obtained while quantification was obtained on ethylene-glycol solvation runs (Moore and Reynolds, 1997). Calcite percentages obtained from XRD measurements were calibrated by calcimetry measurements (Bernard calcimeter, Biogéosciences Laboratory, Université Bourgogne Franche-Comté).

3.5. X-ray fluorescence

X-ray fluorescence (XRF) analyses were conducted on 100 samples taken every 30 cm along the first 33 meters of the section. Each sample was turned into powder and analysed using a

Journal Pre-proof

hand XRF S1 Titan Bruker (Biogéosciences Laboratory, Université Bourgogne Franche-Comté) to identify and quantify major element composition. Analyses of the elementary composition of the shales have been focus on several ratios of chemical elements relevant for approaching the changes in the terrigenous flux (Ti, Fe, Si, Al, K) and indirectly in the grain-size as Si is normally enriched in the silt size fraction and Al and K are commonly enriched in the clay size fraction. We therefore selected the following ratios: Si/Al, Ti/Al, Ti/K and Fe/Al as sedimentological and environmental proxies.

3.6. Spectral analyses

Frequency content analyses were performed using the multi-taper method (MTM; Thomson, 1982, 1990) applying three 2π-tapers (2π-MTM spectra). The confidence levels of the spectral peaks were extrapolated assuming a chi-square distribution of the red-noise fit of the spectral background calculated according to the method of Mann and Lees (1996) implemented in Meyers (2014). The spectra are given with a Rayleigh frequency (frequency resolution of the spectrum) of 0.0099 cycles.m^{-1}. Filters were then calculated using Taner filters (see supplementary material in Hinnov et al., 2002 for technical details of the filter). The sedimentation rate was then calculated per each repetition of the filter of the precession cycle by dividing the thickness of a cycle by the average duration of the precession cycles (20.2 ± 0.5 kyr; Waltham, 2015). We assume that the sedimentation rates are constant within a precession cycle. The TOC series was used as the reference for the precession filter as this series was regularly sampled and shows high amplitude of the filter of the precession throughout the interval studied.

4. Results

Journal Pre-proof

345

346 *4.1. The Huncal section deposits*

347

348 The section is predominantly composed of black shale deposits interrupted by several
349 dolostone interbeds (Figs. 2A, 3). Shale contain abundant ammonites, best preserved in beef
350 and microfossils including radiolarian and coccolithophores. Accumulations of silt-sized
351 quartz grains forming microscopic beds parallel to layering are commonly observed in shale
352 (Fig. 2C). We reported 11 orange-colored competent dolostone beds with sharp contacts
353 ranging from 0.2 m to 1 m thick, which accounts for 5% of the section thickness. Their
354 microfacies is often characterized by an equigranular mosaic of anhedral to subhedral
355 dolomite crystals, probably formed by the postdepositonal diagenesis. This early diagenesis

356

Journal Pre-proof

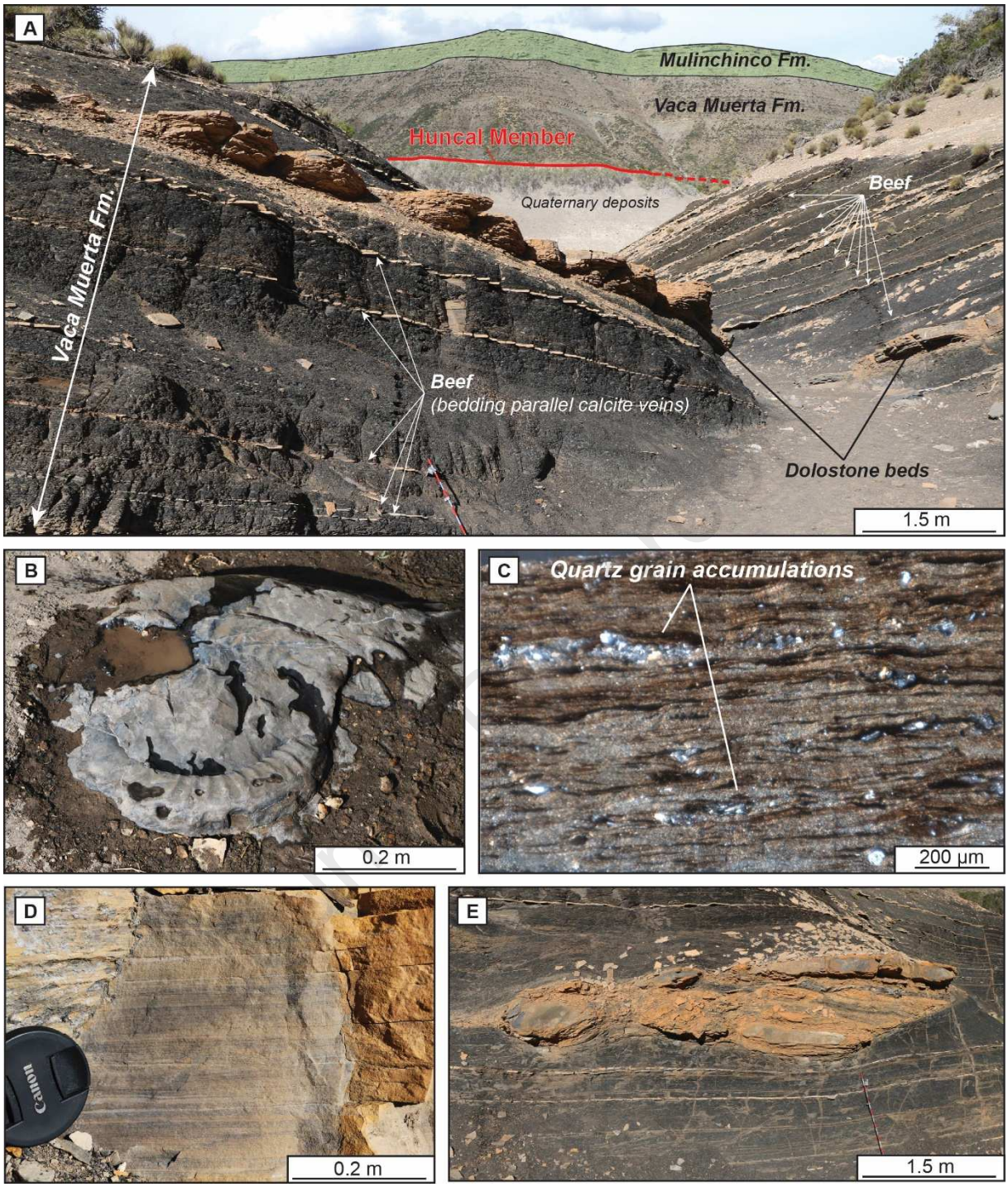


Figure 2. *(A) Typical aspect of the Huncal section where multiple bedding parallel calcite veins (beef) set in the organic-rich mudrock of the Vaca Muerta Fm. Dolostone beds locally interrupt the mudrock lithology. Note the Huncal member position in the upper part of the Vaca Muerta Formation in the background. (B) Ammonite (Catutosphinctes Callomoni) found in a dolostone bed (89 meters). (C) Microscopic view of thinly laminated mudrocks displaying micro-beds composed of silt-sized quartz grains. (D) Thinly laminated dolostone beds that sometimes show faint current ripples. (E) Slump deposits in the Vaca Muerta Fm.*

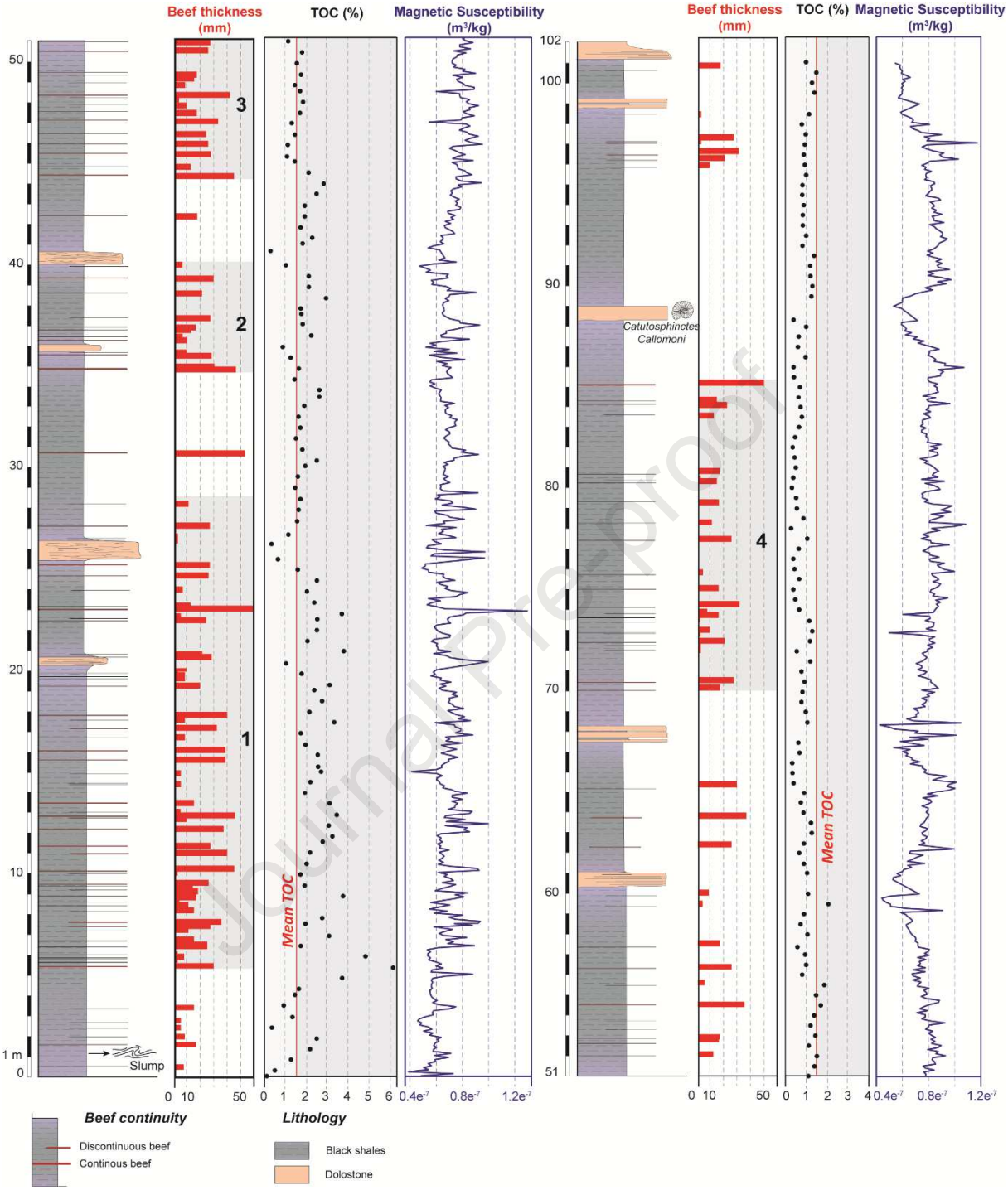


Figure 3. *Sedimentary log of the Huncal section with distribution, thickness and continuity of the beef. TOC values (measured every 50 cm) and MS values (measured every 10 cm) are reported along the section. Shaded intervals labelled 1 to 4 correspond to beef-rich intervals mentioned in the text.*

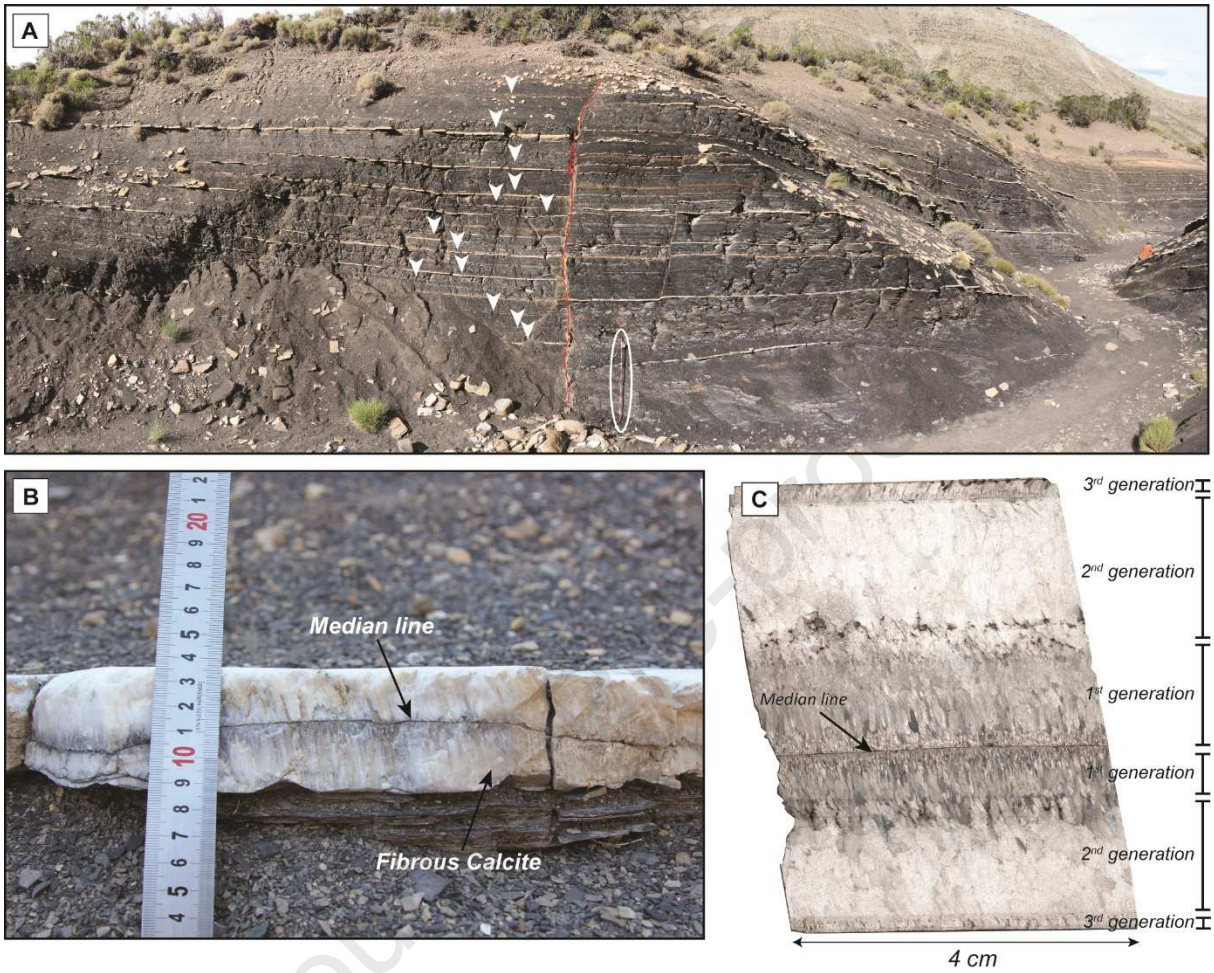
Journal Pre-proof

provides a good preservation of mudstone primary fabric including thinly laminated beds and occasional faint current ripples (Fig. 2D). Thin laminations and current sedimentary structures in a basinal sedimentary succession suggest that dolostones were deposited by very fine-grained sedimentary density flow (Fig. 2B). These beds could either represent the distal part of dilute gravitational flows, perhaps induced by storm surges, turbidites or long-lived muddy hyperpycnal flow originating from the reworking of inner ramp sediments (Spaletti et al., 2000; Blanco et al., 2020) or triggered by extreme river discharges (Otharan et al., 2020). The occurrence of slump deposits at the base of the section (1.2 m) (Fig. 2E) strengthens a gravity-induced origin for these thinly laminated dolostone beds.

4.2. Beef distribution and thickness

Along the section, 135 beef layers have been measured with thickness ranging from 1 to 62 mm (mean thickness: 18 mm) and lateral extent ranging from few meters to tens of meters (Fig. 4A). The cumulated beef thickness accounts for around 4 % of the total thickness of the 102 m thick interval. We measured 16 beef layers comprised between 0 and 2 mm thick, 32 beef between 2 and 10 mm, 34 between 11 and 20 mm, 33 between 21 and 30 mm, 12 between 31 and 40 mm, 7 between 41 and 50 mm and only two being superior to 50 mm thick (Fig. 3). The beef distribution is not homogeneous but clustered in four main stratigraphic intervals ranging from 5 meters up to 26 meters thick (labelled 1 to 4 on Fig. 3). A denser beef proportion is observed in the first 50 meters where the thickest beef layers have also been measured. The first beef-rich interval (5 to 27 meters) gathers 45% of all beef measured along the section (n=61 beef) (Fig. 3). We also observe that intervals with low beef concentration show a few thick beef layers (30.73 m 34.87 m, 62.28 m, 63.74 m, 65.22 m and 85.1 m) (Fig.

394 3). All beef layers show a median line and one to several generations of fibrous calcite
395 crystallisation (Figs. 4B, C).



396
397 ***Figure 4****. (A) Beef-rich intervals in the lower part of the Huncal section (5 to 10 m). White arrows point beef.*
398 *Note 1.5 m Jacob's staff as scale. (B) Close-up on beef structure where a median line separates two sets of*
399 *antitaxial fibrous calcite. (C) Thin section showing beef internal structure characterised by distinctive zones*
400 *related to several generation of fibrous calcite precipitation. The first generation is greyer due to hydrocarbon*
401 *and wall rock inclusion.*

402

403 *4.3. Total Organic Carbon*

404

405 TOC values along the section range from 0.1 to 6.1% along the section with an average of
406 1.5% for the 250 samples measured (Fig. 3). The highest TOC values are measured in the first
407 43 meters where TOC values are mostly above mean TOC. Beef-rich intervals 1 to 3

Journal Pre-proof

generally coincide with higher TOC values (Fig. 3). In the first 33 meters of the section, the occurrences of the thickest beef layers coincide with TOC values above average (Fig. 5).

4.4. Magnetic Susceptibility

MS values range from $0.346.10^{-7}$ to $1.583.10^{-7}$ m^3/kg with an average of $0.734.10^{-7}$ m^3/kg. Mean MS values generally increase in beef-rich intervals and seem to be correlated with the occurrence of thickest beef (Fig. 3, 5).

4.5. Mineralogy of the black shale deposits

X-ray diffraction analyses realized on 125 black shale samples show a mean mineralogical composition characterized by 61% of quartz, 14% of albite, 12 % of clay, 10% of calcite, 2 % of pyrite and less than 1% of gypsum. Calcite percentages obtained from XRD measurements were calibrated by calcimetry measurements. Detailed mineralogical analyses performed in the first 33 meters of the section show similar trend between the Quartz/Clay ratio, used here as a detrital proxy, and the calcite content. The Quartz/Clay ratio displays higher values from 6 to 18 meters (from 1.2 to 1.4; Fig. 5F) while calcite content is the highest between 7 and 20 meters (11 to 14%; Fig. 5E). These two proxies coincide with higher TOC values (2.4% on average) and denser beef distribution (Fig. 5). Pyrite content (ranging from 0 to 22%; 1.3% on average) also displays higher values between 8 and 23 meters with two local maxima around 10 and 20 meters. Clay mineral assemblages show on averages 59% of R3 type illite/smectite mixed-layers (IS R3), 27% of illite, 10% of chlorite and 4% of complex chlorite-vermiculite-smectite mixed-layers. The high proportion of IS R3 (composed of 90% of illite sheets) and

illite indicate that sediments have experienced significant burial diagenesis with a maximal burial temperature of 190°C (Šucha et al.,1993).

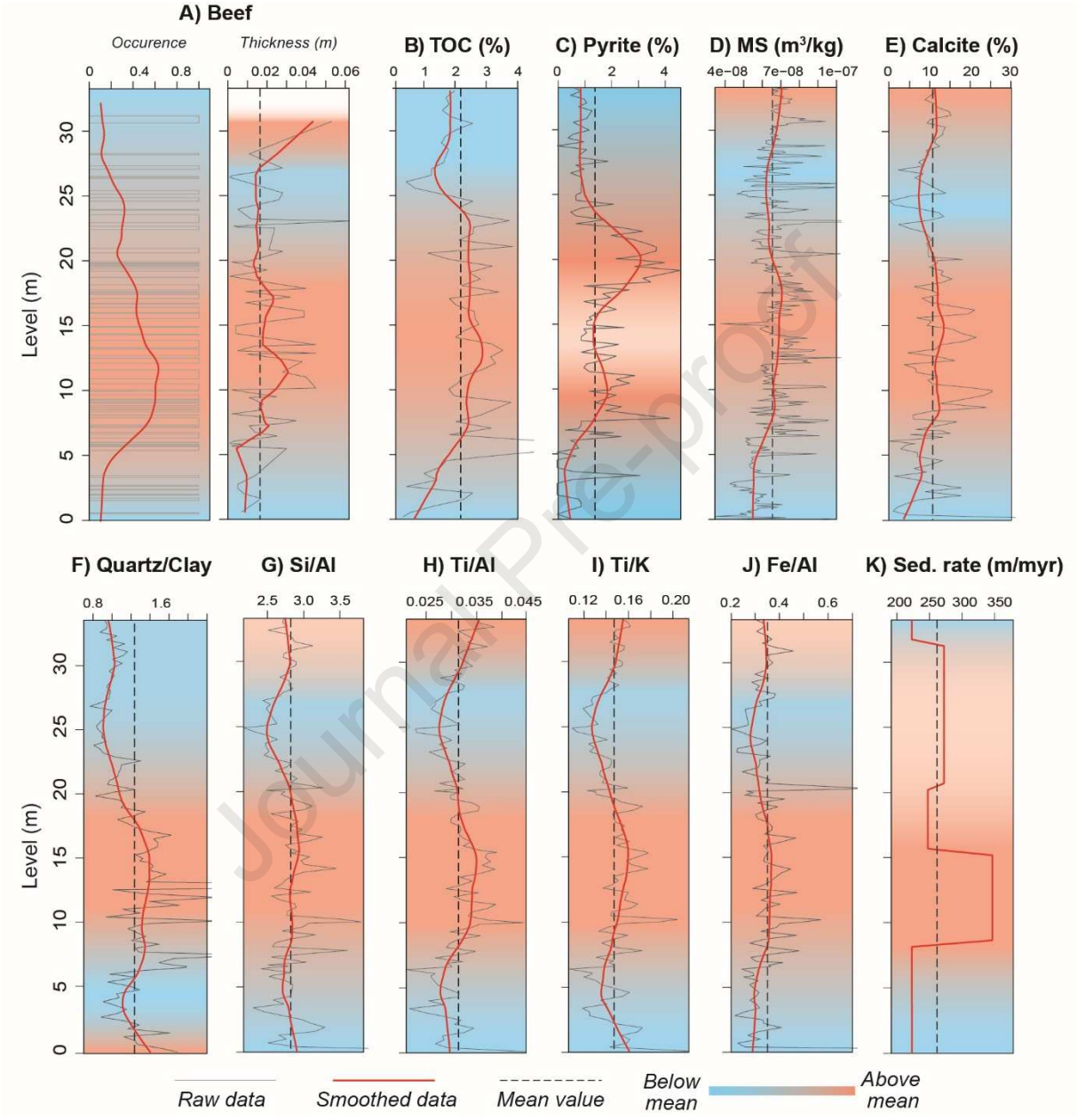


Figure 5. *Evolution of the beef occurrence and thickness, the TOC (every 50 cm), the mineralogical content (Pyrite, Calcite, and Quartz/Clay) and some key ratio of chemical elements (every 30 cm). The sedimentation rate for the first 33 meters of the Huncal section is deduced from the thickness of the precession cycles (cf. section 5.1). Raw and smoothed data are shown for each plot.*

441

442

443

444 *4.6. Geochemistry of the black shale deposits*

445

446 The Si/Al, Ti/Al, Ti/K and Fe/Al ratios display very similar evolution with values above mean
447 reached within the 8 to 19 meters and 29 to 33 meters intervals and below mean in the 0 to 8
448 and 19 to 29 meters intervals (Fig. 5). This evolution positively correlates with other proxies
449 analysed in the first third of the studied section (i.e., beef occurrence and thickness, TOC, MS,
450 Calcite, Quartz/Clay and sedimentation rate).

451

452 *4.7. Spectral analyses*

453

454 The 2π-MTM spectra of the MS, TOC, Beef Occurrence (BO) and Median Beef Position
455 (MBP) series all show three groups of spectral peaks at the following frequencies (Figs. 6, 7
456 and 8):

457 (i) 0.0297 to 0.0396 ± 0.0099 cycles.m^{-1} (corresponding periods: 34 to 25 m),

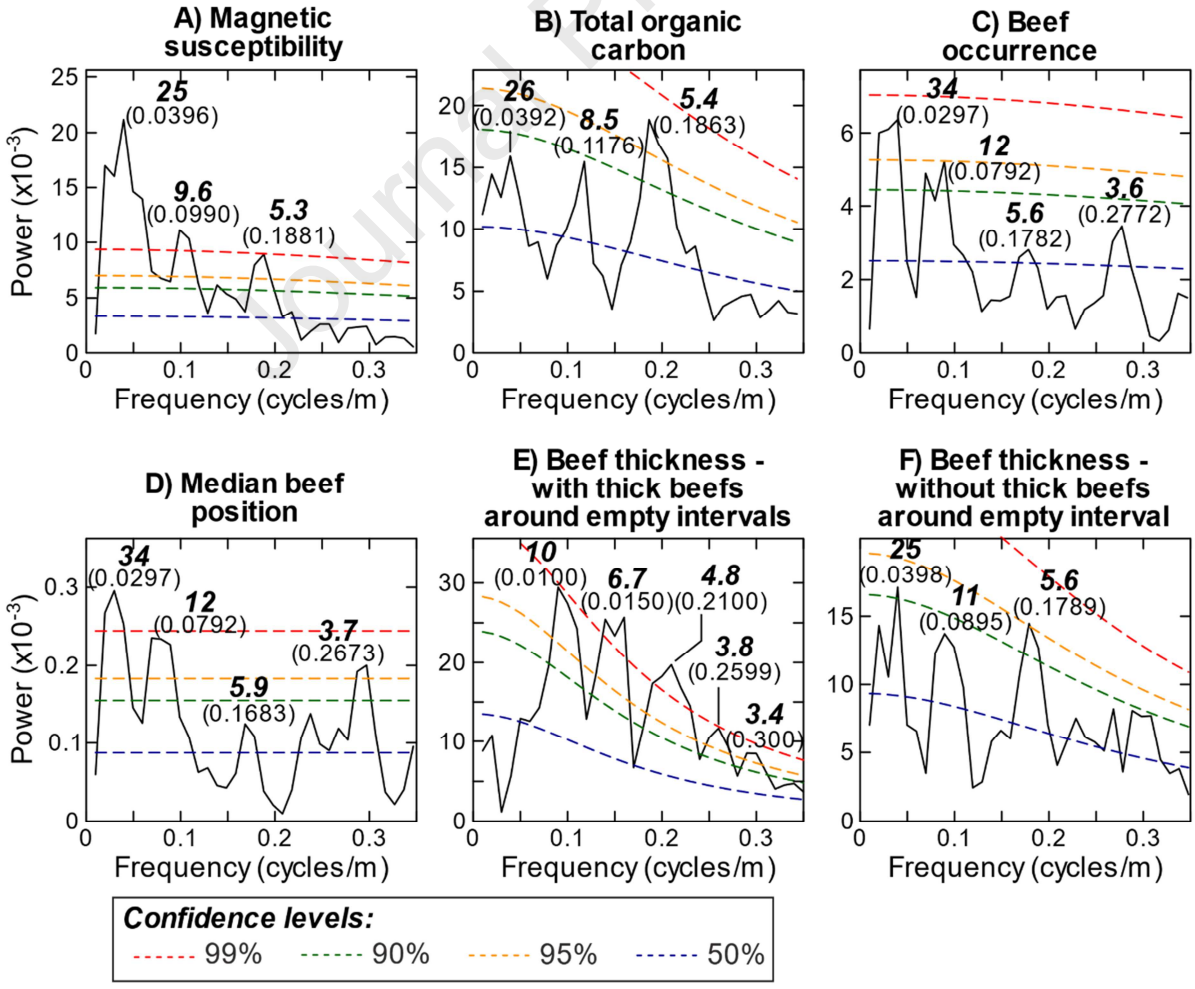
458 (ii) 0.0792 to 0.1275 ± 0.0099 cycles.m^{-1} (corresponding periods: 12 to 8.5 m),

459 (iii) 0.1683 to 0.1881 ± 0.0099 cycles.m^{-1} (corresponding periods: 5.9-5.3 m).

460 The average frequency of these three groups are 0.0346, 0.0938 and 0.1802 cycles.m^{-1},
461 respectively corresponding to periods at 28.9 m, 10.7 m and 5.5 m. Other spectral peaks are
462 observed in the BO and the MBP series respectively at frequencies 0.2772 cycles.m^{-1} (period:
463 3.6 m) and 0.2673 cycles.m^{-1} (period: 3.7 m) (Figs. 6C, 6D and 8).
464 The 2π-MTM spectrum of the Beef Thickness (BT) series shows a group of spectral peaks
465 with decreasing powers from frequencies 0.0100 to 0.300 cycles.m^{-1} (corresponding periods:

from 10.0 m to 3.4 m) (Fig. 6E). At ~30 m, ~60 m and ~90 m, few but thick beef layers are recorded around intervals devoid of beef (see red circles in Fig. 8C), locally creating sequences of high amplitudes. This feature makes the beef thickness series unstationary and biases the spectrum (Weedon, 2003). Interestingly, this pattern occurs recurrently every ~30 m, which corresponds to the longest period observed in the other spectrograms. To overcome this bias, we removed the very thick beefs directly surrounding the intervals devoid of beefs. The beefs discarded from the further analysis are shown as red circles in Figure 8C.

The 2π-MTM spectrum of the BT series without the thick beefs around the intervals devoid of beefs shows spectral peaks at frequencies 0.0398, 0.0895, 0.1789 cycles.m^{-1}, respectively corresponding to 25 m, 11 m and 5.6 m (Fig. 6.F). These periods agree with the periods found in the spectra of the MS, TOC, BO and MBP.



Journal Pre-proof

Figure 6. *2π-MTM spectra of the series measured throughout the entire studied series. Periods of the spectral peaks in meters are labelled bold and are in meters. The corresponding frequencies are labelled in between brackets and are in cycles/m.*

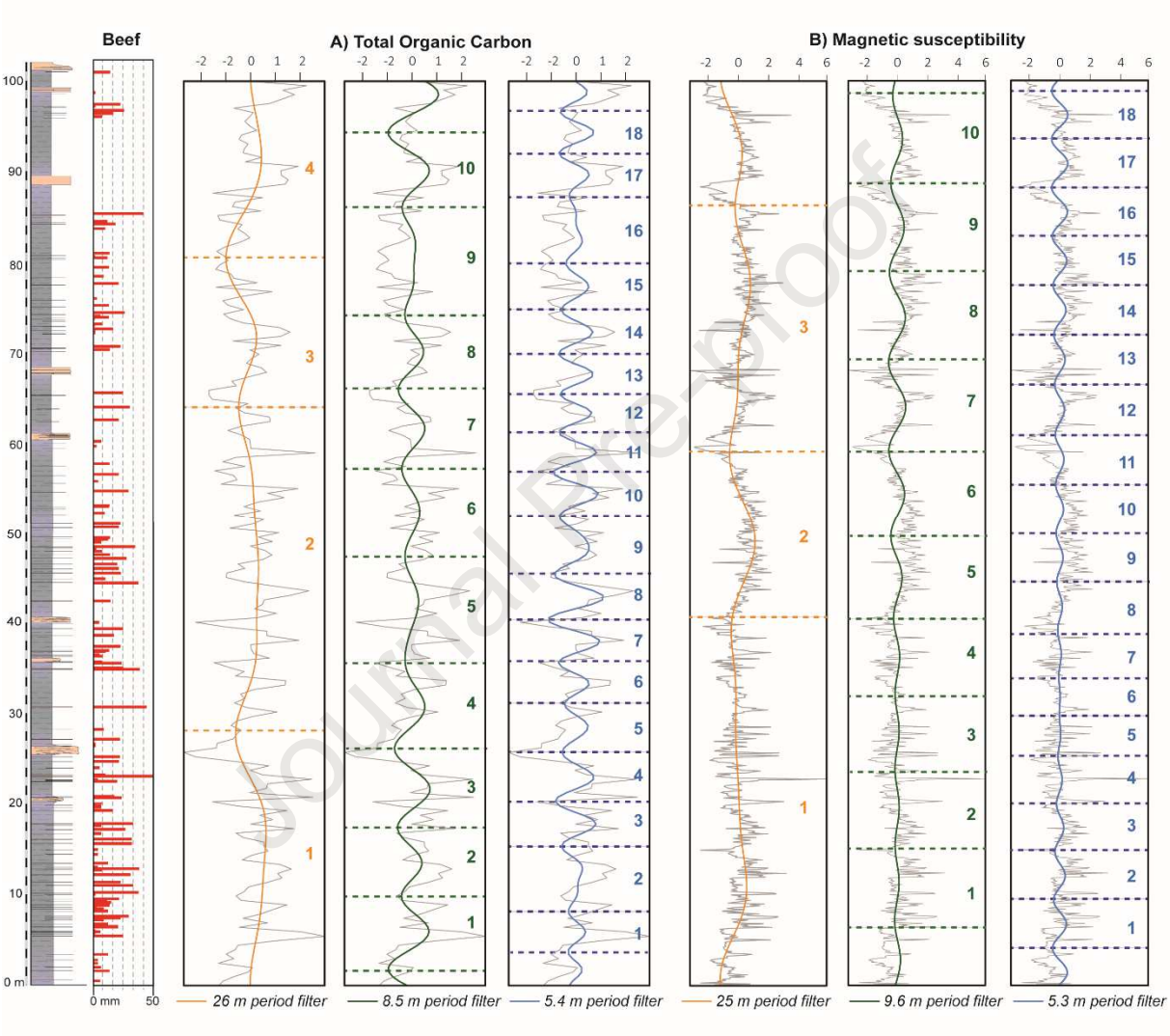
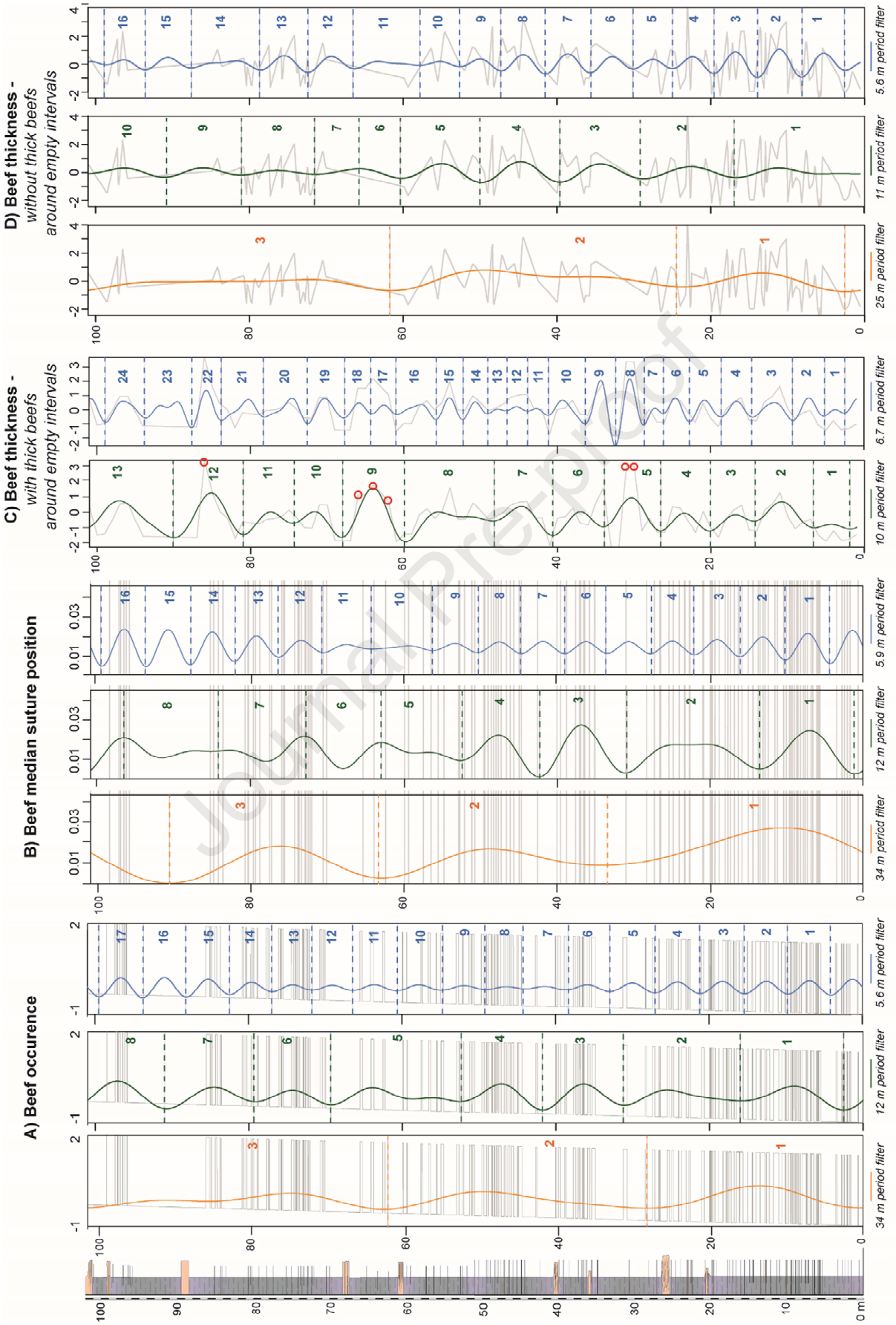


Figure 7. *Taner filters of the Total Organic Carbon (TOC) and the Magnetic Susceptibility (MS) series.*

491


A) Beef occurence
B) Beef median suture position
C) Beef thickness - with thick beefs around empty intervals
D) Beef thickness - without thick beefs around empty intervals
5.6 m period filter
12 m period filter
34 m period filter
5.9 m period filter
6.7 m period filter
10 m period filter
11 m period filter
25 m period filter
0 m

492

Journal Pre-proof

493 ***Figure 8.*** *Taner filters of the beef-related series.*

494

495 **5. Discussion**

496

497 *5.1 Significance of the sedimentary cycles*

498

499 The series of MS, TOC, BO, MBP and BT (without thick beef around intervals devoid of
500 beefs) all display peaks at 25-34 m, 8.5-12 m and at 5.3-5.9 m (Figs. 6, 7 and 8). The
501 difference in the period of the signals is due to the discretisation of the spectra, which is
502 inherent to spectral analyses performed on finite series (Weedon, 2003). This effect is
503 particularly obvious for the longest period, where the ~30 m peak has a period ranging from
504 25 to 34 m depending on the proxy analysed. These peaks have frequencies ranging from
505 0.029 cycles.m^{-1} (34 m) to 0.039 cycles.m^{-1} (25 m). The difference of 0.01 cycles.m^{-1} between
506 these two frequencies corresponds to the frequency resolution of the spectra shown here.
507 On average, three periods are commonly observed between these five above-mentioned
508 proxies, at 28.1 m, 10.8 m and 5.6 m. The ratio between these periods is 1.9:2.6:5.0, in perfect
509 agreement with the ratios between the periods of 100 kyr (eccentricity), 38.1 kyr (obliquity)
510 and 20.2 kyr (average precession) (Waltham, 2015). The observed periods of ~28 m, 11 m
511 and 5.6 m are thus respectively associated to the eccentricity, the obliquity and the precession,
512 which appears to influence both the lithological characteristics (TOC, MS) and mineralization
513 produced during diagenesis (beef distribution and thickness) of the Vaca Muerta deposits.
514 The spectrum of the BT does not show these periods when including the thick beefs around
515 intervals devoid of beefs (Fig. 6E). However, as demonstrated in section 4.2, this series is
516 biased as it only shows high powers localised at intervals where few but thick beefs occur. It
517 is noteworthy that these thick beef intervals occur every ~30 m, which corresponds to the
518 100-kyr eccentricity in the spectra of TOC, MS, BO and MBP. This shows that eccentricity

Journal Pre-proof

519 cycles impacted mudstone properties, so that it favoured the generation of thick, isolated beef
520 layers in organic-depleted intervals. After removing these beefs at 30.73 m 34.87 m, 62.28 m,
521 63.74 m, 65.22 m and 85.1 m (see red circles in Fig. 8C), the spectrum of the BT series
522 displays the same peaks at 25 m, 11 m and 5.6 m observed in the other proxies and related to
523 the imprint of the eccentricity, obliquity and precession, respectively. Notice that the different
524 beef signals display other peaks at 3-4 m which are not observed in the MS or TOC signals.
525 As they are not observed in other environmental proxies, these short periods observed in the
526 beef-related series are likely due to specific burial and diagenetic processes rather than the
527 imprint of an environmental change.
528
529 *5.2. Astroclimatic fingerprint and beef distribution model*
530
531 Detailed mineralogical and chemical analyses performed along the Huncal section show that
532 increasing beef density and thickness correlate with higher MS, TOC, calcite content, silt-to-
533 clay ratios and sedimentation rate (Fig. 5). This correlation suggests a link between the
534 primary sedimentary signal, diagenesis and hydrofracturing distribution in the mudrocks of
535 the Vaca Muerta Fm. Similar relationships have been proposed by other studies focusing on
536 the mechanisms of beef formation (Rodrigues et al., 2009; Zanella et al., 2015; Meng et al.,
537 2017; Larmier, 2020) although astroclimatic precursors have hitherto remained unexplored.
538 Based on spectral analyses, we demonstrate the influence of the orbital parameters as a
539 precursor for variations in both sedimentary signals (MS, TOC) and diagenetic features
540 (beef). Beef distribution can therefore be deciphered by considering the evolution of the
541 sedimentary record in view of climatic and/or eustatic fluctuations inferred from orbital
542 parameters.

Journal Pre-proof

Krim et al. (2017, 2019) suggested that grain-size and clay mineralogy variations observed in the southern part of the Neuquén Basin during deposition of Vaca Muerta Fm can be considered as a climatic imprint rather than a response to eustatic variations. Warm temperate conditions associated with seasonal rainfall and increase runoff are proposed to explain the increase of siliciclastic supply recorded in the Vaca Muerta mudrocks (Scasso et al., 2005; Krim et al., 2019). Clay mineralogy is commonly used as a proxy for climatic reconstructions (humidity/aridity) in the Late Jurassic (Hallam 1993; Pellenard & Deconinck 2006; Pellenard et al., 2014; Turner & Huggett 2019) and was used in this way at a regional scale for the Vaca Muerta Fm (Krim et al., 2019). Unfortunately, temperatures reached by the Huncal section during the burial diagenesis (~ 190°C; Mean Tmax = 590°C) strongly affected mineralogy of clays, mainly composed of illite, IS R3 and chlorite, preventing the use of clay minerals as proxy of climate and comparison with the paleoenvironmental signal deduced from the south of the Neuquén Basin (i.e., Huincul Arch area; Krim et al., 2019).

However, periods of increased sedimentary flux and siliciclastic supply, in relation with enhanced runoff conditions during wetter climate are here supported by high ratios of Quartz/Clay, Si/Al, Ti/Al, Ti/K and Fe/Al in the lower Huncal section that coincide with a high sedimentation rate deduced from the thickness of the precession cycles (~ 300 $m.myr^{-1}$) (Figs. 5 and 9A). Enhanced runoff and detrital export also correlate with an augmentation of the TOC and iron content in the mudrocks (Fig. 5). Increased sedimentation rate and seawater fertilization during wetter conditions can explain the positive feedback observed for the TOC content in response to better organic matter preservation and increased primary productivity (Arthur et al., 1987; Scasso et al., 2005; Armstrong et al., 2016). Classically in the Mesozoic, organic-rich deposits become widespread at time of acceleration of the hydrolysing cycle during more humid period (Dera et al., 2009; Föllmi, 2012; Martinez and Dera, 2015). Otharan et al. (2020) also relate the high organic matter content in the Vaca Muerta mudrocks

Journal Pre-proof

to the basinward increase of detrital flux during humid periods through deposition of long-lived muddy hyperpicnal flows triggered by extreme rivers discharges. Organic matter incorporation during basinward transport and fast deposition could have enhanced organic matter preservation and accumulation. In other locations of the basin, variations in TOC content in the Vaca Muerta Fm have been related to palaeoproductivity during marine transgression (highest TOC values) or dilution processes during marine regression (lowest TOC values), combined with fluctuations of the redox conditions due to episodic restriction of water-mass circulation (Kietzmann et al., 2016; Krim et al., 2017, 2019). The climatic-driven model proposed here is not mutually exclusive with the role of eustatism evoked by Kietzmann et al. (2016) in the coeval fluctuations in primary productivity, calcite export to the sea bottom and the detrital input. Organic-rich mudrocks with an enhanced detrital fraction are commonly encountered in transgressive phases in the Neuquén Basin (Kietzmann et al., 2016) implying that orbitally-driven sea level fluctuations may have influenced the lithological characteristics of the mudrocks and therefore the rheology and beef distribution of the Vaca Muerta Fm. The very homogenous clayey lithology of the Vaca Muerta Fm encountered in the Huncal area and the reduced window of observations and sampling (100 m-thick section) prevent the role of eustatism in controlling sedimentary cycles to be further discussed.

At the Jurassic-Cretaceous boundary, a growing aridity evidenced by large evaporate deposits coupled with clay mineralogical, palynological or numerical modelling data is worldwide recorded (Hallam, 1982; Valdes et al., 1995; Price et al., 1997; Schnyder et al., 2006; Sellwood and Valdes, 2008; Krim et al., 2017; Cameille et al., 2018; Turner & Huggett 2019). Sedimentary intervals recording reduced sedimentation rate (< 250 $m.myr^{-1}$) and lower values of Quartz/Clay, Si/Al, Ti/Al, Ti/K and Fe/Al ratios may indicate periods of decrease in runoff related to more arid climatic conditions (Fig. 9B). Reduced siliciclastic supply is also

combined to a decrease in mean TOC (from 2.4% to 1.7%). Fluctuations in runoff and sedimentary flux recorded in the Huncal area could also be related to latitudinal migration of the climatic belts as proposed by Sagasti (2005) and Krim et al. (2017) for the lower Cretaceous of the Neuquén Basin. Fluctuations in terrigenous supply to the basin occurred also likely in response to alternating climate regimes from arid to temperate depending on the configuration of the Earth's orbit (Sagasti, 2005). Similar conditions have also been suggested to occur during Late Jurassic times (Valdes et al., 1995, Armstrong et al., 2016).

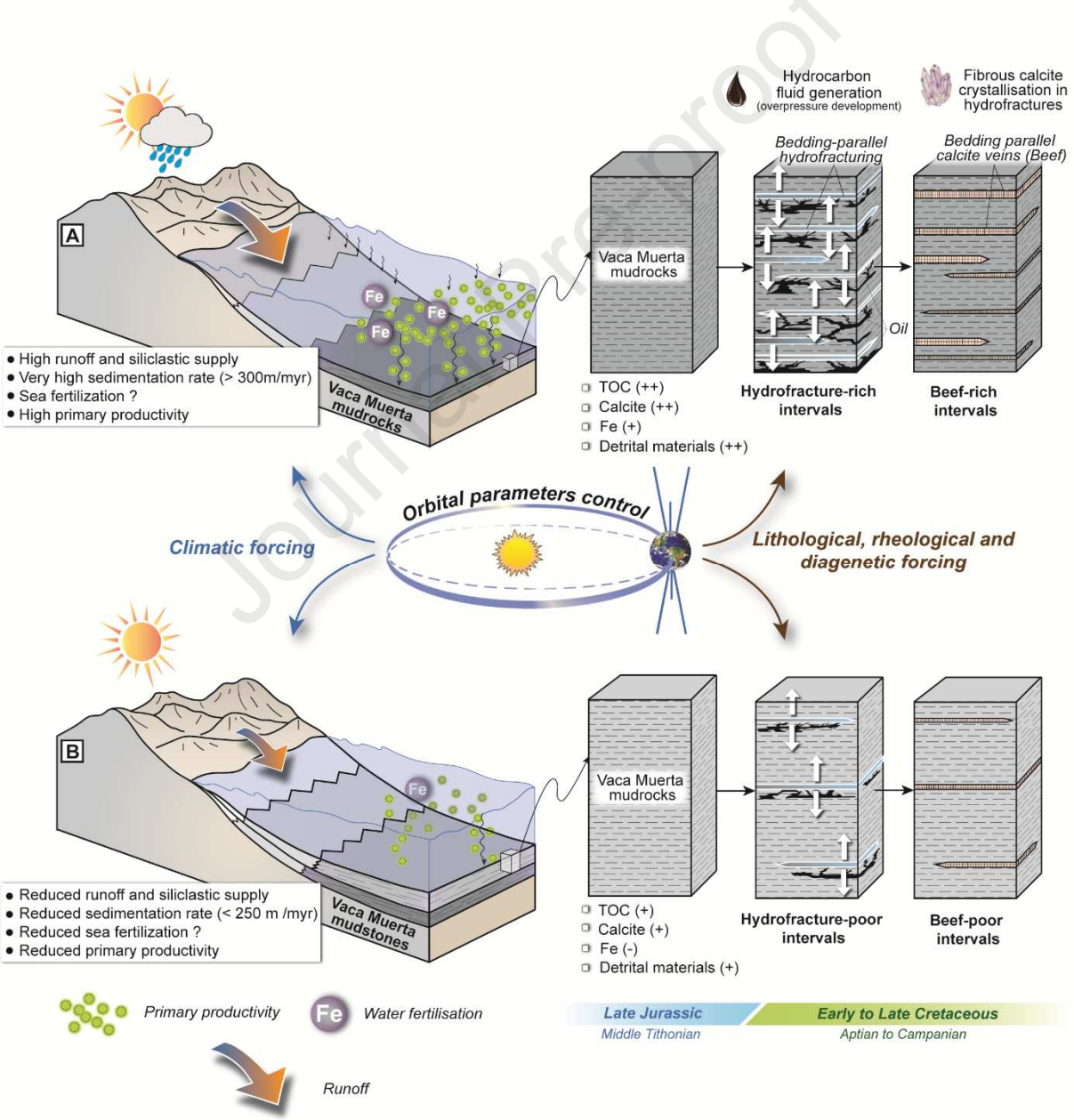


Figure 9. *Astroclimatic model for the Late Jurassic Vaca Muerta Fm in the Huncal area and its control on lithology and diagenesis. (A) Semi-arid conditions: higher runoff, siliclastic supply, TOC and sedimentation*

Journal Pre-proof

rate. Organic-rich black shale facies favors the development of beef-rich intervals during diagenesis by abundant hydrocarbon generation and subsequent hydrofracturing during the Cretaceous (Rodrigues et al., 2009). (B) More arid conditions: Reduced runoff, siliclastic supply, TOC and sedimentation rate. The reduction of organic content in black shales coincides with beef-poor intervals because of a decrease in hydrocarbon and hydrofracture generation during diagenesis. Transitions between arid and semi-arid conditions are most certainly related to latitudinal fluctuations of climatic belts in response to changes of the orbital parameters.

Calcite content is surprisingly positively correlated with TOC values, sedimentation rate and increased siliciclastic supply. The opposite trend was observed in the Chos Malal area, north of the Huncal area, with a negative correlation between TOC and calcite content (Kietzmann et al., 2015; Rodriguez Banco et al., 2020). In this area, clear alternations between black shales and limestone outcrop. The limestone beds there are interpreted as carbonate mud produced in the platform and exported to the basin via density cascading currents (Rodriguez Blanco et al., 2020). In the Huncal section, very few calciturbidite beds are intercalated within a thick dark bituminous shale series. The increasing calcite content could correspond to the enhanced preservation of calcareous bio-grains content in mudstones, in the conditions of a TOC content predominantly influenced by palaeoproductivity. Alternatively, carbonate authigenesis might explain the unpredictable correlation between TOC values, calcite content and sedimentation rates. Authigenic calcium carbonate precipitation represents a non-negligible component of the global carbon cycle that is thought to be enhanced where the organic matter delivery to the sea floor is likely to be high (Sun and Turchyn, 20140). Miliken et al. (2019) show evidence of radiolarian calcitization and demonstrate a correlation between high TOC values and the precipitation of calcite during diagenesis of the Vaca Muerta mudrocks north of the Huncal area. The localised presence of diffuse beef measuring less than a millimetre, referred to as “microbeef” in Lejay et al. (2017) could have also been incorporated into mudrock samples analysed in this study, possibly explaining the positive

Journal Pre-proof

correlation between TOC and calcite content. Although diagenesis might influence the calcite content measured in shales from the Huncal section, Milliken et al. (2019) suggest that characteristics of the diagenesis are primary controlled by the depositional setting, thus explaining the relation between calcite content, TOC, sedimentation rates and Earth's orbital parameters we establish in this study. We therefore propose that periodic fluctuations in humidity/aridity have influenced sedimentary and biogenic processes that control any lithological and rheological variations recorded in the black shales of the Huncal area (Fig. 9). Paleoclimatic fluctuations have left an indelible fingerprint on the sedimentary record today highlighted by the distribution of diagenetic features (e.g. beef) as demonstrated along the Huncal section. This astroclimatic fingerprint on beef distribution could partially be obliterated in some other sections of the Vaca Muerta Fm displaying beef-rich intervals, especially where some relations between ash beds, fossils or calcitic concretions and beef distribution have been evidenced (Rodrigues et al., 2009; Lejay et al., 2017; Weger et al., 2019). Knowing that ash beds and concretions are very sparse in the studied section and that lithology is rather homogeneous along the deciphered interval, most mechanical contrasts and discontinuities used for hydrofracturing propagation derive from minor but recurrent changes in sedimentary characteristics (detrital fraction, TOC) inherited from astroclimatic forcing we demonstrated above. Based on these results, we suggest that the Milankovitch fingerprint on beef distribution has certainly a best potential for preservation in basinal sections characterized by high sedimentation rate, homogeneous lithology and low concentration of mechanical contrasts inherited from aerial explosive volcanism and/or diagenesis.

6. Conclusion

Journal Pre-proof

We demonstrate that the Milankovitch cyclicity rule the processes controlling the composition of organic-rich sediments in the basinal part of the Neuquén Basin. The relations and cycles inferred from the statistical treatment of sedimentary (MS, elemental and mineralogical ratios), biogenic (TOC) and diagenetic (beef distribution and thickness) signals revealed the influence of the astroclimatic fingerprint recorded in sediments on processes controlling mineralized fracture generation and distribution. During burial (probably once catagenesis started), carbonate- and organic-rich sediments emplaced during enhanced wetter conditions favoured the development of a dense bedding-parallel network of mineralised fractures along weaker rheological plans. By slightly modifying the lithological and rheological characteristics of the black shales deposited in the basin, reduced runoff and drier conditions might have been the precursor explaining the occurrence of beef-poor intervals in the Huncal section. Knowing the importance of mechanical discontinuities during hydraulic-fracture stimulation, the astroclimatic memory recorded in the distribution of mineralized fracture could help predicting the density of discontinuities in source rocks using a suitable mix of mineralogical and geochemical proxies coupled to cyclostratigraphic signal analyses following Milankovitch theory.

Journal Pre-proof

Acknowledgement

This study is part of the CYCLOBEEF project funded by “Institut National des Sciences de L’Univers” through the programme Tellus and CESSUR (Connaissance et technologie du Sous-Sol pour son exploitation et usage durable) action. The authors would like to thank Salomé Larmier and Régis Mourgues for their contributions and discussions on the field and Hector Leanza for his help in ammonoids determination. Matthieu Branellec is

Journal Pre-proof

thanked for the drawing of the beautiful geological map of the Neuquén Basin. We also want to thank Jean-François Deconinck and François Baudin for their constructive remarks during the elaboration of the project. Ludovic Bruneau is thanked for his contribution in XRD and XRF measurements and Christelle Gruber is also thanked for the production of thin sections.

References

Arthur, M.A., Zachos, J.C., Jones, D.S., 1987. Primary productivity and the Cretaceous/Tertiary boundary event in the oceans. Cretaceous Research 8, 43–54. https://doi.org/10.1016/0195-6671(87)90011-5.

Aguirre-Urreta, B., Martinez, M., Schmitz, M., Lescano, M., Omarini, J., Tunik, M., Kuhnert, H., Concheuro, A., Rawson, P.F., Ramos, V.A., Reboulet, S., Noclin, N., Frederichs, T., Nickl, A.L., Pälike, H., 2019. Interhemispheric radio-astrochronological calibration of the time scales from the Andean and the Tethyan areas in the Valanginian–Hauterivian (Early Cretaceous). Gondwana Research 104, 104–132. https://doi.org/10.1016/j.gr.2019.01.006.

Armstrong, H.A., Wagner, T., Herringshaw, L.G., Farnsworth, A.J., Lunt, D.J., Harland, M., Imber, J., Loptson, C., Atar, E.F., 2016. Hadley circulation and precipitation changes controling black shale deposition in the Late Jurassic Boreal Seaway. Paleoceanography 31, 1041–1053. https://doi.org/10.1002/2015PA002911.

Carmeille, M., Bourillot, R., Brunet, M. F., Pellenard, P., Fürsich, F. T., Schnyder, J., Barrier, E., Blanpied, C., Sidorova, I., 2018. Architecture and sedimentary evolution of the southwestern Gissar carbonate platform (Uzbekistan) during the Middle–Late Jurassic. Marine and Petroleum Geology 97, 437–465. https://doi.org/10.1016/j.marpetgeo.2018.07.021.

Journal Pre-proof

706 Cobbold, P.R., Rodrigues, N., 2007. Seepage forces, important factors in the formation of horizontal
707 hydraulic fractures and bedding-parallel fibrous veins ('beef' and 'cone-in-
708 cone'). Geofluids 7, 313–322. https://doi.org/10.1111/j.1468-8123.2007.00183.x.

709 Cobbold, P.R., Zanella, A., Rodrigues, N., Løseth, H., 2013. Bedding-parallel fibrous veins (beef and
710 cone-in-cone): Worldwide occurrence and possible significance in terms of fluid overpressure,
711 hydrocarbon generation and mineralization. Marine and Petroleum Geology 43, 1–20.
712 https://doi.org/10.1016/j.marpetgeo.2013.01.010.

713 Cosgrove, J.W., 1995. The expression of hydraulic fracturing in rocks and sediments. Geological
714 Society, London, Special Publications 92, 187–196.
715 https://doi.org/10.1144/GSL.SP.1995.092.01.10.

716 Dera, G., Pellenard, P., Neige, P., Deconinck, J.F., Pucéat, E., Dommergues, J. L., 2009. Distribution
717 of clay minerals in Early Jurassic Peritethyan seas: palaeoclimatic significance inferred from
718 multiproxy comparisons. Palaeogeography, Palaeoclimatology, Palaeoecology 271, 39–51.
719 https://doi.org/10.1016/j.palaeo.2008.09.010.

720

721 Eberli, G.P., Weger, R.J., Tenaglia, M., Rueda, L., Rodriguez, L., Zeller, M., McNeil, D., Murray, S.,
722 Swart, P., 2017. The Unconventional Play in the Neuquén Basin, Argentina–Insights From the
723 Outcrop for the Subsurface, in: Unconventional Resources Technology Conference, Austin,
724 Texas, 24-26 July 2017 (pp. 2208-2219). Society of Exploration Geophysicists, American
725 Association of Petroleum Geologists, Society of Petroleum Engineers.
726 https://doi.org/10.15530/URTEC-2017-2687581.

727

728 Föllmi, K.B., 2012. Early Cretaceous life, climate and anoxia. Cretaceous Research 35, 230–257.
729 https://doi.org/10.1016/j.cretres.2011.12.005.

730

731 Franzese, J.R., Spalletti, L.A., 2001. Late Triassic-early Jurassic continental extension in southwestern
732 Gondwana: tectonic segmentation and pre-break-up rifting. Journal of South American Earth

Journal Pre-proof

Sciences 14, 257–270. https://doi.org/10.1016/s0895-9811(01)00029-3.

Gale, J.F.W., Laubach, S.E., Olson, J.E., Eichhubl, P., Fall, A., 2014. Natural fractures in shale: A review and new observations. AAPG Bulletin 98, 2165–2216. https://doi.org/10.1306/08121413151.

Garrido, A.C., Parent, H., Brambilla, L., 2018. Tithonian stratigraphy and ammonite fauna of the Vaca Muerta Formation in Mallín Quemado (Neuquén Basin, Argentina), with remarks on the Andean chronostratigraphy. Volumina Jurassica 16, 1-26. https://doi.org/10.5604/01.3001.0012.0496.

Grauls, D. 1999. Overpressures: Causal mechanisms, conventional and hydromechanical approaches. Oil & Gas Science and Technology-Revue D IFP Energies Nouvelles 54, 667–678. https://doi.org/10.2516/ogst:1999056.

Hallam, A., 1982. The Jurassic climate, in: Berger, W.H., Cromwell, J.C. (Eds.), Studies in Geophysics: Climate in Earth History. National Academy Press, Washington, DC, 159–163.

Hallam A., 1994. Jurassic climates as inferred from the sedimentary and fossil record, in: Allen J.R.L., Hoskins B.J., Sellwood B.W., Spicer R.A., Valdes P.J. (Eds.), Palaeoclimates and their Modelling. Springer, Dordrecht, 79–88. https://doi.org/10.1007/978-94-011-1254-3_10.

Hinnov, L.A., 2018. Cyclostratigraphy and Astrochronology in 2018, in: Montenari, M. (Ed.), Stratigraphy and Timescales vol. 3: Cyclostratigraphy and Astrochronology, 1–80. https://doi.org/ 10.1016/bs.sats.2018.08.004.

Journal Pre-proof

Hinnov, L.A., Schulz, M., Yiou, P., 2002. Interhemispheric space-time attributes of the Dansgaard-Oeschger oscillations between 0-100 ka. Quaternary Science Reviews 21, 1213–1228. https://doi.org/10.1016/S0277-3791(01)00140-8.

Howell, J.A., Schwarz, E., Spalletti, L.A., Veiga, G.D., 2005. The Neuquen Basin: an overview, in: Veiga, G.D., Spalletti, L.A., Howell, J.A., Schwarz, E. (Eds.), The Neuquén Basin, Argentina: A Case Study in Sequence Stratigraphy and Basin Dynamics, Geological Society, London, Special Publications 252, 1–14. https://doi.org/10.1144/gsl.sp.2005.252.01.01.

Hunt, C.P., Moskovitz, B.M., Banerjee, S.K., 1995. Magnetic Properties of Rocks and Minerals, in: Ahrens, T.J. (Ed.), Rock Physics and Phase Relations: A Handbook of Physical Constants. AGU Reference Shelf 3, American Geophysical Union, Washington DC, 189–204. https://doi.org/10.1029/RF003p0189.

Kietzmann, D.A., Palma, R.M., Riccardi, A.C., Martín-Chivelet, J., López-Gómez, J., 2014. Sedimentology and sequence stratigraphy of a Tithonian-Valanginian carbonate ramp (Vaca Muerta Formation): A misunderstood exceptional source rock in the Southern Mendoza area of the Neuquen Basin, Argentina. Sedimentary Geology 302, 64–86. https://doi.org/10.1016/j.sedgeo.2014.01.002.

Kietzmann, D.A., Palma, R.M., Iglesia Llanos, M.P., 2015. Cyclostratigraphy of an orbitally-driven Tithonian-Valanginian carbonate ramp succession, Southern Mendoza, Argentina: Implications for the Jurassic-Cretaceous boundary in the Neuquen Basin. Sedimentary Geology 315, 29–46. https://doi.org/10.1016/j.sedgeo.2014.10.002.

Kietzmann, D.A., Ambrosio, A.L., Suriano, J., Alonso, M.S., Tomassini, F.G., Depine, G., Repol, D.,

Journal Pre-proof

2016. The Vaca Muerta–Quintuco system (Tithonian–Valanginian) in the Neuquén Basin, Argentina: A view from the outcrops in the Chos Malal fold and thrust belt. AAPG Bulletin 100, 743–771. https://doi.org/10.1306/02101615121.

Kietzmann, D.A., Iglesia Llanos, M.P., Kohan Martínez, M., 2018. Astronomical Calibration of the Tithonian–Berriasian in the Neuquén Basin, Argentina: A Contribution From the Southern Hemisphere to the Geologic Time Scale, in: Montenari, M. (Ed.), Stratigraphy and Timescales 3, Cyclostratigraphy and Atrochronology, 327–355. https://doi.org/10.1016/bs.sats.2018.07.003.

Kohan Martínez, M., Kietzmann, D.A., Iglesia Llanos, M.P., Leanza, H.A., Luppo, T. 2018. Magnetostratigraphy and cyclostratigraphy of the Tithonian interval from the Vaca Muerta Formation, southern Neuquen Basin, Argentina. Journal of South American Earth Sciences 85, 209–228. https://doi.org/10.1016/j.jsames.2018.05.010.

Krim, N., Bonnel, C., Tribovillard, N., Imbert, P., Aubourg, C., Riboulleau, A., Bout-Roumazeilles, V., Hoareau, G., Fasentieux, B., 2017. Paleoenvironmental evolution of the southern Neuquén basin (Argentina) during the Tithonian-Berriasian (Vaca Muerta and Picun Leufu Formations): a multi-proxy approach. BSGF - Earth Sciences Bulletin 188, 34. https://doi.org/10.1051/bsgf/2017196.

Krim, N., Tribovillard, N., Riboulleau, A., Bout-Roumazeilles, V., Bonnel, C., Imbert, P., Aubourg, C., Hoareau, G., Fasentieux, B., 2019. Reconstruction of palaeoenvironmental conditions of the Vaca Muerta formation in the southern part of the Neuquén Basin (Tithonian-Valanginian): Evidences of initial short-lived development of anoxia. Marine and Petroleum Geology 103, 176-201. https://doi.org/10.1016/j.marpetgeo.2019.02.011.

Larmier, S., 2020. Génération de fluides, migration et fracturation au sein des roches mères : cas de

Journal Pre-proof

la formation de Vaca Muerta, bassin de Neuquén, Argentine (PhD Thesis) Le Mans Université, Le Mans (507 pp.).

Laskar, J., Fienga, A., Gastineau, M., Manche, H., 2011. La2010: a new orbital solution for the long-term motion of the Earth. Astronomy and Astrophysics532, A89. https://doi.org/ 10.1051/0004-6361/201116836.

Leanza, H.A., Hugo, C.A., Repol, D., Salvarredy Aranguren, M., 2003. The Huncal Member (Lower Berriasian): a turbidite episode in the Vaca Muerte Formation, Neuquén basin, Argentina. Miembro Huncal (Berriasiano inferior): un episodio turbidítico en la Formación Vaca Muerta, Cuenca Neuquina, Argentina. Revista de la Asociación Geológica Argentina 58, 248–254.

Leanza, H.A., Sattler, F., Martínez, R., Carbone, O., 2011. La Formación Vaca Muerta y Equivalentes (Jurásico Tardío–Cretácico Temprano) en la Cuenca Neuquina. Geología y Recursos Naturales de la Provincia del Neuquén, Neuquén. Buenos Aires. Revista de la Asociación Geológica Argentina, 113–129.

Legarreta, L., Gulisano, C.A., 1989. Análisis estratigráfico secuencial de la Cuenca Neuquina (Triásico superior-Terciario inferior, Argentina), in: Chebli, G., Spalletti, L.A. (Eds.), Serie Correlación Geológica 6, Cuencas Sedimentarias Argentina, Universidad Nacional de Tucumán, Tucumán, 221–243.

Legarreta, L., Uliana, M.A., 1991. Jurassic—Marine Oscillations and Geometry of Back-Arc Basin Fill, Central Argentine Andes, in: Macdonald, D.I.M (Ed.), Sedimentation, Tectonics and Eustasy: Sea-Level Changes at Active Margins, Special Publication of the International Association of Sedimentologists 12, Blackwell Scientific Publications, Oxford, 429-450. https://doi.org/10.1002/9781444303896.ch23.

Journal Pre-proof

Lejay, A., Larmier, S., Rutman, P., & Gelin, F., 2017. The Role of Porosity in the Development of Parallel Bedded Calcite Filled Fractures (or Beef) in the Vaca Muerta: An Integrated Analysis From High Resolution Core Data. In *Unconventional Resources Technology Conference, Austin, Texas, 24-26 July 2017* (pp. 394-409). Society of Exploration Geophysicists, American Association of Petroleum Geologists, Society of Petroleum Engineers.

Martinez, M., Dera, G., 2015. Orbital pacing of carbon fluxes by a ~9-My eccentricity cycle during the Mesozoic. Proceedings of the National Academy of Sciences 112, 12604–12609. https://doi.org/10.1073/pnas.1419946112.

Meng, Q., Hooker, J., Cartwright, J., 2017. Early overpressuring in organic-rich shales during burial: evidence from fibrous calcite veins in the Lower Jurassic Shales-with-Beef Member in the Wessex Basin, UK. Journal of the Geological Society 174, 869–882. https://doi.org/10.1144/jgs2016-146.

Meng, Q., Hooker, J., Cartwright, J., 2018. Role of pressure solution in the formation of bedding-parallel calcite veins in an immature shale (Cretaceous, southern UK). Geological Magazine 156, 918–934. https:// doi:10.1017/S0016756818000377.

Meyers, S. R., 2014. Astrochron: An R Package for Astrochronology (Version 0.3)

Milankovitch, M., 1920. Théorie mathématique des phénomènes thermiques produits par la radiation solaire. Gauthier-Villars, Paris.

Milliken, K.L., Reed, R. M., McCarty, D. K., Bishop, J., Lipinski, C.J., Fischer, T.B., Crousse, L., Reijenstein, H., 2019. Grain assemblages and diagenesis in the Vaca Muerta Formation (Jurassic-

Journal Pre-proof

869 Cretaceous), Neuquén Basin, Argentina. *Sedimentary Geology 380*, 45–64.
870 https://doi.org/10.1016/j.sedgeo.2018.11.007.

871

872 Moore, D.M., Reynolds, R.C., 1997. X-Ray Diffraction and the Identification and Analysis of Clay
873 Minerals, 2nd edition. Oxford University Press, Inc., New York.

874

875 Otharán, G.A., Zavala, C., Arcuri, M., Di Meglio, M., Zorzano, A., Marchal, D., Köhler, G., 2020.
876 Facies analysis of organic-rich fluid mud flow deposits. The lower section of the Vaca Muerta
877 Formation (Tithonian) at basinal positions, Neuquén Basin, Argentina. Andean Geology 47,
878 384-417. http://dx.doi.org/10.5027/andgeoV47n2-3061.

879

880 Pellenard P., Deconinck J.-F., 2006. Mineralogical variability of Callovo-Oxfordian clays from the
881 Paris Basin and the Subalpine Basin. Comptes Rendus Geoscience 338, 854–866.
882 https://doi.org/10.1016/j.crte.2006.05.008.

883

884 Pellenard, P., Tramoy, R., Pucéat, E., Huret, E., Martinez, M., Bruneau, L., Thierry, J., 2014. Carbon
885 cycle and sea-water palaeotemperature evolution at the Middle–Late Jurassic transition,
886 eastern Paris Basin (France). Marine and Petroleum Geology 53, 30–43.
887 https://doi.org/10.1016/j.marpetgeo.2013.07.002.

888

889 Petschick, R., 2001. MacDiff: the user-friendly x-ray powder diffractometry analysis tool for
890 Macintosh computers.

891

892 Parent H., Garrido A.C., Scherzinger A., Schweigert G., Fözy I., 2015. The Tithonian-Lower
893 Valanginian stratigraphy and ammonite fauna of the Vaca Muerta Formation in Pampa Tril,
894 Neuquén Basin, Argentina. Boletín del Instituto de Fisiografía y Geología 86, 1–96.

895

Journal Pre-proof

Price, G.D., Valdes, P.J., Sellwood, B. W., 1997. Quantitative palaeoclimate GCM validation: Late Jurassic and mid-Cretaceous case studies. Journal of the Geological Society 154, 769–772. https://doi.org/10.1144/gsjgs.154.5.0769.

Ramos, V. A., Naipauer, M., Leanza, H. A., & Sigismondi, M. E., 2019. The Vaca Muerta Formation of the Neuquén Basin: An Exceptional Setting along the Andean Continental Margin. AAPG Memoir 120 Vaca Muerta Fm.

Riccardi, A., 2015. Remarks on the Tithonian-Berriasian ammonite biostratigraphy of west central Argentina. Volumina Jurassica 13, 23–52.

Rodrigues, N., Cobbold, P.R., Loseth, H., Ruffet, G., 2009. Widespread bedding-parallel veins of fibrous calcite (’beef') in a mature source rock (Vaca Muerta Fm, Neuquén Basin, Argentina): evidence for overpressure and horizontal compression. Journal of the Geological Society 166, 695–709. doi.org/10.1144/0016-76492008-111.

Rodriguez Blanco, L., Eberli, G.P., Weger, R.J., Swart, P.K., Tenaglia, M., Rueda Sanchez, L.E., McNeill, and D.F., 2020. Periplatform ooze in a mixed siliciclastic-carbonate system - Vaca Muerta Formation, Argentina. Sedimentary Geology 396, 105521.

Sagasti, G., 2005. Hemipelagic record of orbitally-induced dilution cycles in Lower Cretaceous sediments of the Neuquén Basin. Geological Society, London, Special Publications 252, 231–250. https://doi.org/10.1144/GSL.SP.2005.252.01.11.

Scasso, R.A., Alonso, M.S., Lanés, S., Villar, H.J., Laffitte, G., 2005. eochemistry and petrology of a Middle Tithonian limestone-marl rhythmite in the Neuquén Basin, Argentina: depositional and burial history. Geological Society, London, Special Publications 252, 207–229. https://doi.org/10.1144/GSL.SP.2005.252.01.10.

Journal Pre-proof

Schnyder, J., Ruffell, A., Deconinck, J.-F., Baudin, F., 2006. Conjunctive use of spectral gamma-ray logs and clay mineralogy in defining late Jurassic–early Cretaceous palaeoclimate change (Dorset, UK). Palaeogeography, Palaeoclimatology, Palaeoecology, 229, 303–320. https://doi.org/10.1016/j.palaeo.2005.06.027.

Sellwood, B.W., Valdes P.J., 2008. Jurassic climates. Proceedings of the Geologists Association 119, 5–17. https://doi.org/10.1016/s0016-7878(59)80068-7.

Spalletti, L.A., Franzese, J.R., Matheos, S.D., Schwarz, E., 2000. Sequence stratigraphy of a tidally dominated carbonate-siliciclastic ramp; the Tithonian-Early Berriasian of the Southern Neuquén Basin, Argentina. Journal of the Geological Society 157, 433–446. https://doi.org/10.1144/jgs.157.2.433.

Strasser, A., Hilgen, F.J., Heckel, P.H., 2006. Cyclostratigraphy – concepts, definitions, and applications. Newsletters on Stratigraphy 42, 75–114. https://doi.org/10.1127/0078-0421/2006/0042-0075.

Sucha, V., Kraus, I., Gerthofferova, H., Petes, J., Serekova, M., 1993. Smectite to illite conversion in bentonites and shales of the East Slovak Basin. Clay Minerals 28, 243–243. https://doi.org/10.1180/claymin.1993.028.2.06.

Sun, X., Turchyn, A.V., 2014. Significant contribution of authigenic carbonate to marine carbon burial. Nature Geoscience 7, 201–204. https://doi.org/10.1038/ngeo2070.

Swarbrick, R.E., Osborne, M.J., 1998. Mechanisms that generate abnormal pressures: an overview, in: Law B.E., Ulmishek G.F., Slavin V.I. (Eds.), Abnormal pressures in hydrocarbon environments. American Association of Petroleum Geologists Memoir 70, 13–34.

Journal Pre-proof

Thomson, D.J., 1982. Spectrum Estimation and Harmonic-Analysis. Proceedings of the IEEE 70, 1055–1096. https://doi.org/10.1109/PROC.1982.12433.

Thomson, D.J., 1990. Quadratic-Inverse Spectrum Estimates: Applications to Paleoclimatology. Philosophical Transactions of the Royal Society of London Series a-Mathematical Physical and Engineering Sciences 332, 539–597. https://doi.org/10.1098/rsta.1990.0130.

Turner, H.E., Huggett, J.M., 2019. Late Jurassic–Early Cretaceous climate change record in clay minerals of the Norwegian-Greenland Seaway. Palaeogeography, Palaeoclimatology, Palaeoecology, 534, 109331. https://doi.org/10.1016/j.palaeo.2019.109331.

Ukar, E., Lopez, R.G., Laubach, S.E., Gale, J.F.W., Manceda, R., Marrett, R., 2017. Microfractures in bed-parallel veins (beef) as predictors of vertical macrofractures in shale: Vaca Muerta Formation, Agrio Fold-and-Thrust Belt, Argentina. Journal of South American Earth Sciences 79, 152–169. https://doi.org/ 10.1016/j.jsames.2017.07.015.

Valdes, P.J., Sellwood, B.W., Price, G.D., 1995. Modelling Late Jurassic Milankovitch climate variations, in: House, M.R., Gale, A.S. (Eds.), Orbital Forcing Timescales and Cyclostratigraphy, Geological Society, London, Special Publications 85, pp. 115–132. https://doi.org/10.1144/GSL.SP.1995.085.01.07.

Vennari, V.V., 2016. Tithonian ammonoids (cephalopoda, Ammonoidea) from the Vaca Muerta Formation, Neuquén basin, west-central Argentina. Palaeontographica Abteilung A, 85 –165. https://doi.org/10.1127/pala/306/2016/85.

Vergani, G.D., Tankard, A.J., Belotti, H.J., Welsink, H.J., 1995. Tectonic evolution and paleogeography of the Neuquén Basin, Argentina, in: Tankard, A.J., Suarez Soruco, R.

Journal Pre-proof

977 Welsink, H.J. (Eds.), Petroleum Basins of South America, AAPG Memoirs 62, 383–402.
978 https://doi.org/10.1306/M62593C19.
979
980 Waltham, D., 2015. Milankovitch period uncertainties and their impact on cyclostratigraphy. Journal
981 of Sedimentary Research 85, 990–998. https://doi.org/10.2110/jsr.2015.66**.**
982
983 Weedon, G.P., 2003. Time-Series Analysis and Cyclostratigraphy, Cambridge University Press,
984 Cambridge.
985
986 Weger, R.J., Murray, S.T., McNeill, D.F., Swart, P.K., Eberli, G.P., Blanco, L.R., Rueda, L., 2019.
987 Paleo thermometry and distribution of calcite beef in the Vaca Muerta Formation, Neuquén
988 Basin, Argentina. AAPG Bulletin 103, 931–950. https://doi.org/10.1306/10021817384**.**
989
990 Zanella, A., Cobbold, P.R., Boassen, T., 2015a. Natural hydraulic fractures in the Wessex Basin, SW
991 England: Widespread distribution, composition and history. Marine and Petroleum
992 Geology 68, 438-448. https://doi.org/10.1016/j.marpetgeo.2015.09.005.
993
994 Zanella, A., Cobbold, P. R., Ruffet, G., & Leanza, H. A., 2015b. Geological evidence for fluid
995 overpressure, hydraulic fracturing and strong heating during maturation and migration of
996 hydrocarbons in Mesozoic rocks of the northern Neuquén Basin, Mendoza Province,
997 Argentina. Journal of South American Earth Sciences 62, 229–242.
998 https://doi.org/10.1016/j.jsames.2015.06.006.
999
1000 Zanella, A., Cobbold, P. R., Rodrigues, N., Loseth, H., Jolivet; M., Gouttefangeas, F., Chew, D., 2020.
1001 Source rocks in foreland basins: a preferential context for the development of natural hydraulic
1002 fractures. AAPG Bulletin.
1003

Journal Pre-proof

Zeiss, A., Leanza, H.A., 2010. Upper Jurassic (Tithonian) ammonites from the lithographic limestones of the Zapala region, Neuquén Basin, Argentina. Berringeria 41, 25–75.

Zhang, J., Jiang, Z., Jiang, X., Wang, S., Liang, C., & Wu, M., 2016. "Oil generation induces sparry calcite formation in lacustrine mudrock, Eocene of east China. Marine and Petroleum Geology 71, 344–359. https://doi.org/10.1016/j.marpetgeo.2016.01.007.

Journal Pre-proof

Journal Pre-proof

Highlights

- Times-series analyses on sedimentary proxies and diagenetic calcite veins (beef)
- Milankovitch cycles controlled detrital input and preservation of organic matter
- Imprint of the Milankovitch cycles on the reccurence and thickness of beef
- Initial climate forcing induces differential diagenesis and control beef distribution in source rocks

Journal Pre-proof

Journal Pre-proof

Declaration of interests

☒ The authors declare that they have no known competing financial interests or personal relationships that could have appeared to influence the work reported in this paper.

☐The authors declare the following financial interests/personal relationships which may be considered as potential competing interests:

Journal Pre-proof